Towed-ROV

Semester report in Mechatronics

Author's: Jonas Halle, Endre Myhre and Jørgen Ringdal Sæter

Aalesund, November 2020

Supervisors: Guoyuan Li, Ottar Laurits Osen

Norwegian University of Science and Technology
Faculty of Engineering
Department of Ocean Operations and Civil Engineering

NTNU
Norwegian University of Science and Technology

Abstract

An ROV was built with the intention to adjust its depth to a given value whilst towed by a boat. Collected sensor data is processed to drive stepper motors to separately rotate two wings via a geared transmission system. Measurements of water column pressure decide the depth position. Initially, the assignment was to improve an ROV already built, however, its condition appeared to be too poor to use at sea, thus a new design was preferable. Here we show a waterproof ROV design with a possibility to assign depths within the range of seven to thirteen meters below the surface at its current settings. We found that the hydrofoil design of the wings and its connection to the transmission system has more impact on performance than previously assumed, and that a PID controller is efficient for depth control. Our prototype has been able to perform as wanted in a limited capacity and is adding insight for future improvements. This ROV prototype is not finely tuned, and there is still room for improvements in both design and software. While giving a vessel to continue research on, it has also provided numerous ideas to enhance performance and simplify production in future versions.

Acknowledgement

We would like to thank the people who have contributed and helped us throughout this project:

- Ottar Laurits Osen - for guidance throughout the project.
- Guoyuan Li - for guidance throughout the project.
- Houxiang Zhang - for guidance in the beginning of the project.
- Lars Petter Bryne - for guidance in the beginning of the project.
- Karl Henning Halse - for guidance in the beginning of the project.
- Anders Sætersmoen and the lab assistants - for help with acquiring materials and lending us hardware.
- Lars Ivar Hatledal - for guidance with AGX simulation.
- Vilmar Æsøy - for guidance during mould production and casting polyurethane.
- Andre Tranvåg and the mechanical apprentices for providing materials, and machining the shaft system

Contents

List of Tables

List of Figures

Chapter 1

Introduction

1.1 Previous work

The towed-ROV was first built in 2018 for a bachelor project, and was modified by two consecutive groups. The project is inspired by The Acrobat from Sea Science Inc, shown in figure 1.1. The design of the ROV have been changed a couple of times, while the materials have been the same.The previous group managed to control the ROV manually, but due to bad weather and a pushing deadline there where some lack in testing.

Figure 1.1: [5] The Acrobat

1.2 Objectives

For this project we wanted to build an ROV that are more robust in terms of waterproofness and mechanical motion. With a control system that can keep it at a constant depth. The physical system, the velocity and size of the wings must be in proportion to each other. We hope to acquire enough testing data to either prove that the system is working, or at least find the issues and prepare the ROV for future work. As there have been a lot of people involved over the last three years, there might be time for some refactoring of the software. There have been some issues with the quality of the pictures and video taken, so we will implement a new camera hoping for some better results.

1.2.1 Improvements

The assignment given was to improve the existing ROV. We went for inspection and concluded that the ROV was not in a condition that would allow us to take it on a sea trial. Most of the oil in the compartments were spilled, and in the previous report they wrote that there were some water entering the boxes the last time they tested the ROV. For this reason we wanted to build an ROV in a more solid material, with no risk of breaking the ROV when opening and closing flanges. There were also more backlash in moving mechanisms than acceptable, allowing the wings to rotate about 10 degrees with the motors in a locked position. The last big improvement we wanted to make was to develop a working control system for depth. As none of the previous groups have been able to do sufficient testing, it's not possible for us to compare with previous results.

1.2.2 Potential use of the ROV

The ROV is well suited for missions that demands under water covering of great areas at a low cost. There are several potential tasks where the ROV can contribute.

Search

In the event of a sunken ship or aircraft the towed ROV can be quite effective in search over large areas. The main advantage for a towed ROV is that it don't operate with a limited power supply.

Measurement

For low budget research the towed rov can be useful for collecting data. The ROV should have an easy to use interface, making it possible for the researchers to connect the sensors needed.

Sea floor mapping

As the ROV is cheap, and can operate over large distances. It should be ideal for mapping the seafloor with pictures. This can be useful for research, but also a good way to enlighten people about pollution etc.. There are already some interests for the ROV to find objects that should be removed from the ocean, so divers can go to the same location.

Chapter 2

Methods and material

2.1 ROV BODY introduction

The body is the enclosure and attachment point of every component in the ROV. It's the part that travels in the water and is impacted by turbulence and currents. Every difference in shape on the body is a potential cause for turbulence that change the hydrodynamic behaviour of the ROV.

Our objective was to create a body that was not allowing any seawater to enter. Also, it should not be necessary to fill up the body with rapeseed oil like the previous version while operating in modest depths. As the rapeseed oil would extend the time spent on any simple change or fix within the body.

When constructing waterproof equipment that also needs to withstand pressure differences, one should keep possible leakage points to a minimum. We would prefer an offshore camera to avoid having to make another waterproof container, but the camera available to NTNU Ålesund was vacant at the time of constructing. A camera placement within the hull would be a substantial weak point.

We gathered all the other components to one single hull with a manhole opening based on the flange standard of DN200. The manhole opening allows for good accessibility to every component. Stainless M16 nuts and stud-bolts allow for mounting and dismounting the manhole flange many times without wearing out threads.

2.2 Body selection

The previous versions of the ROV were mostly made out of acrylic plastic plates, with some aluminium angle bars for support. Acrylic plastic plates are simple to

cut to wanted shapes in a CNC laser cutter, and the density makes the weight nearly neutral in seawater. However, the mechanical properties of this type of plastic is a substantial weakness in a construction for this purpose. Acrylic plastic plates are vulnerable when subjected to compressive forces and twists. When inspecting the previous ROV, there were obvious cracks in several bolt holes. Many of the cracks were clearly a cause for rapeseed oil leakage. It was used a sanitary silicone in the plastic plate joints, and the hold was weak. Silicone does not stick well to plastics and hardened silicone. Silicone joints can't be patched. However, one would have to remove all hardened silicone and make new joints. Rubber gaskets caused flexing in the flanges when tightening the bolts. We suspect cracking in the flange lids was due to this.

An alternative to constructing is to buy commercially made enclosures for underwater applications. This would considerably reduce the time spent on construction. Spending much time constructing before testing for results is a risk in this type of project. Buying commercially could also help with solutions for opening and closing the enclosure in a simpler way, built with manufacturing methods not available at NTNU Ålesund. However, in a mass-produced product, it's likely to be difficult to fit custom components like shaft penetrations. If the enclosure was going to be custom made to our needs, the time waiting for the product might not pay off, and the price is likely to have increased.

By building ourselves from our own design, we could keep the working pace according to a plan. Changes and unforeseen challenges could be dealt with as the building went on. The ROV would have to be made in a weldable and machinable material. Weldable plastics were ruled out because of the need for considerable greater wall thicknesses and a resulting added weight when welding and machining than metals. When welding plastics like for example polyethylene, tacks cant be made to build up the construction before fully welding, however one would need hold the parts at the desired spot and then and fully weld. Keeping the accuracy to an acceptable result would be time consuming. Steel is a strong and durable material, and wall thicknesses down to 1mm are doable even in high pressures. However, if any other component needs to be welded to the body, it has to be steel. If this component happens to need a bulkier body, the weight will increase dramatically. A weldable aluminium alloy would allow us to add more material in welding without a substantial weight increase. Aluminium welds warp and pull far less than steel. Aluminium is simpler to machine, wears less on tools, and is not as sensitive for feeds and speeds as steel, making the production faster. On the other hand, aluminium is more subjected to wear than steel if handled a lot. Aluminium threads wears out easily, which is a challenge with prototyping. Having a plan and thinking through every mount was necessary.

2.2.1 Design

The ROV body is inspired by the previous design of square containers of components with side plates working as fins, and high wing placement for stability. The previous and new design is shown in figures 2.1 and 2.2.

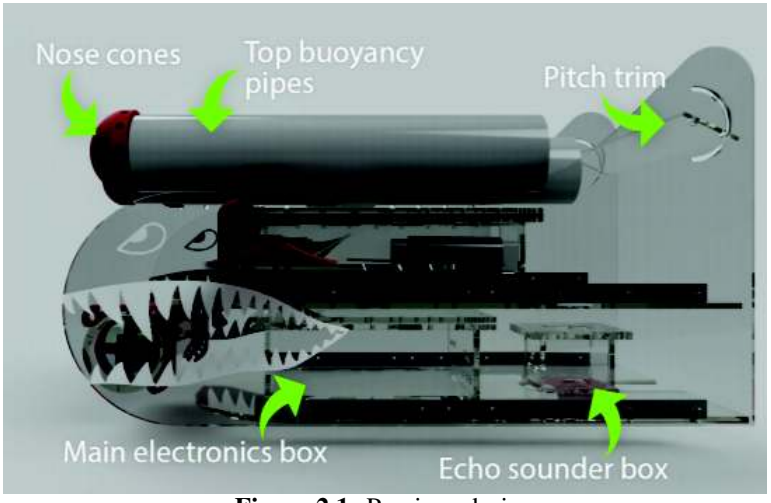

Figure 2.1: Previous design

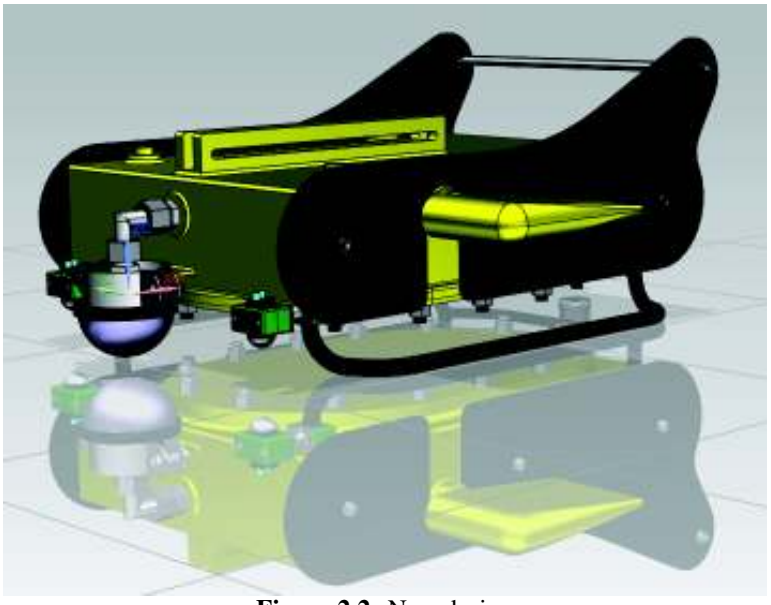

Figure 2.2: New design

Two 20mm aluminium pipes were bent and welded to the hull to make legs. The pipes make it easier to carry the ROV and protect the ROV-body, floors and substrates. A smaller pipe was bent and welded between the two leg pipes on the back

of the ROV. The echo sounder's original bracket was welded to this pipe.

The two plastic side plates were cut with a CNC laser. The side plates are simple to mount and dismount with three stud bolts and nuts each. It's also simple to produce new plates in different shapes. A stainless spoiler is mounted between the plates. The spoiler is fixed and functions more like a plate stiffener at this point. More testing is needed to determine the spoilers effect on the ROV, and possibly introduce motor steering later.

The camera housing is placed in the ROV's front. Ideally, the front would be more hydrodynamic customized. However, with the need for an external waterproof camera housing, it was a solution allowing us to keep up the building pace, with the possibility to improve the shape of the front later.

The towing cable's attachment point allows for moving the cable's shackle along the length of the ROV's top half. The attachment point was milled manually and welded to the body. An M12 carriage bolt and nut are easily loosened to slide to the desirable point.

2.3 Building and solutions

Body

After figuring out the internal space needed for electronics, shafts, gears and motors, a 3D-model of the body was designed in Siemens NX. 2D DWG files were exported of each plate. The DWG files contained holes for wing- and motor-placements. The DWG files were sent to a company who CNC water jet cut aluminium plates. The plates were welded together. Different sized sockets for sensors, cable penetrations and wing shafts were machined and welded to the body.

Welding

TIG welding is the optimum method when welding 6mm plates to a waterproof box. When designing the box, the plates were offset by their own thickness to create natural V-groove joints all around. TIG welding allows for full control when filling the groove with filler material. Special attention can be given to places with weld tacks and bigger gaps in the joint when TIG welding.

Aluminium TIG welding is a different technique than TIG welding steel. Heat radiates more in aluminium, and the filler is not as eager to fuse with the workpiece. Aluminium is dependent on thoroughly clean surfaces when welding. Exposed surfaces on aluminium will develop an aluminium oxide film. Welds do not fuse to aluminium oxide, so it needs to be cleaned off. An aluminium weld bead is likely to have internal voids if the welder is not systematically filling up the groove,

keeping a tight arc, and making sure of fully melted penetration the full length of the joint. Also, the filler rod tip is dependent on gas coverage under welding. When keeping this in mind when welding, one will most of the time end up with good looking beads and no need for patching.

The manhole flange, having more than three times the thickness than the other parts, needed preheating before welding. Parts with different wall thicknesses concentrates heat differently. Using a cutting torch with an acetylene and oxygen mix, the flange was preheated. The preheat is concentrated mostly on where the welding is going to start because heat travels along as the weld goes on. However, heat must be added all over the part to avoid radiation away from the weld.

Camera housing

The camera needed a waterproof enclosure. A plastic transparent bulb with a plastic loose flange was provided. The loose flange was intended to be sealed with an O-ring on the counter-flange. An aluminium shaft was turned in the lathe to the bulb's flange diameter and an internal space to accept the camera and servo motor. To get an O-ring groove in the aluminium flange, a custom HSS tool would have to be made for the lathe. To save time, and reduce the risk of needing to scrap the part due to failure, a cork gasket was made to replace the O-ring sealant. Cork was used because it deforms to the surfaces between the two flanges and doesn't cause flex in the plastic flange as bolts are tightened like rubber. Also, cork does not require the same pressure to seal like a fibre gasket. The camera- and servo motor was mounted on a simple 3D- printed installation.

The camera enclosure was attached to the ROV body with stainless steel clamps, and the camera- and servo motor cable entered the ROV body through a pipe filled with epoxy. We used Ermeto high-pressure fittings for this pipe which allows for easy removal if another camera is wanted later. The socket welded to the ROV-body has internal 3/4"BSP threads.

Cable penetration

Sockets for every cable penetration was turned and threaded manually. Holes were drilled at the desired positions on the hull, and the sockets were welded. The lights, echo sounder and pressure sounder, all had commercial made cable penetrations, M10 external threads and a hollow inside filled with a soft epoxy.

The towing cable's penetration was custom made. A hole two times the diameter of the cable diameter was drilled through a stainless 1"BSP plug. On the seaside part of the plug, a bigger drill was partially drilled in. This made a conical shape that would help the epoxy handle more of the forces made from water pressure.

The lights commercial made cable penetration also needed an epoxy refill. The towing cable's penetration, the lights penetration and camera ermeto pipe were prepped for epoxy casting by passing through the desired cable length and by sealing the end pointing away from the sea. We used sanitary silicone to seal the ends. A two-component epoxy usually used for coating was provided. The epoxy was mixed, poured, and left to harden overnight.

Pipe bending

The 20mm pipes used for the legs were bent in a pipe bending machine. The first pipe was bent by feel, up and around the flange to not imperil the access to the nuts. The other pipe was copied from the first. The pipes were then welded to ROV.

When bending pipes, it's important to slightly over-bend the desired bending angle due to the natural suspension of the material. The suspension varies with different materials and wall thicknesses.

Shaft and shaft penetration

Figure 2.3: 3D model of shaft solution

The wing shaft system shown in figur 2.3, is the ROVs weak point in regards to water resistance because of rotation both inside and outside of the hull. The shafts are not subjected to high angular velocities or loads, yet the construction should not be too compact for easy machining. The two bearings on each shaft have an ID of 12mm, and OD of 21mm. Both bearings are 61801-2RS1 produced by SKF. This bearing has contact seals on both sides.

The shafts are turned out of stainless steel. Both bearings are press-fitted to the shaft. Both ends of the shaft are threaded to external M6 for mounting of gear and wing flange. Figure 2.4 shows the technical drawing made in Autocad.

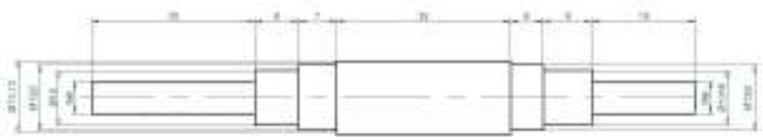

Figure 2.4: Technical drawing of shaft

The shaft penetration is turned out of aluminium. The bearings are also press-fitted to the hub. Simple custom tools were made in the lathe to press-fit to shaft

and hub on both bearings. After pressing one of the bearings on shaft and hub, the penetration was filled with propeller shaft grease before pressing the other bearing. The seaside of the wing shaft system was then filled with more grease, and a spring-loaded shaft seal was pressed on. Figure 2.5 shows the technical drawing made in Autocad.

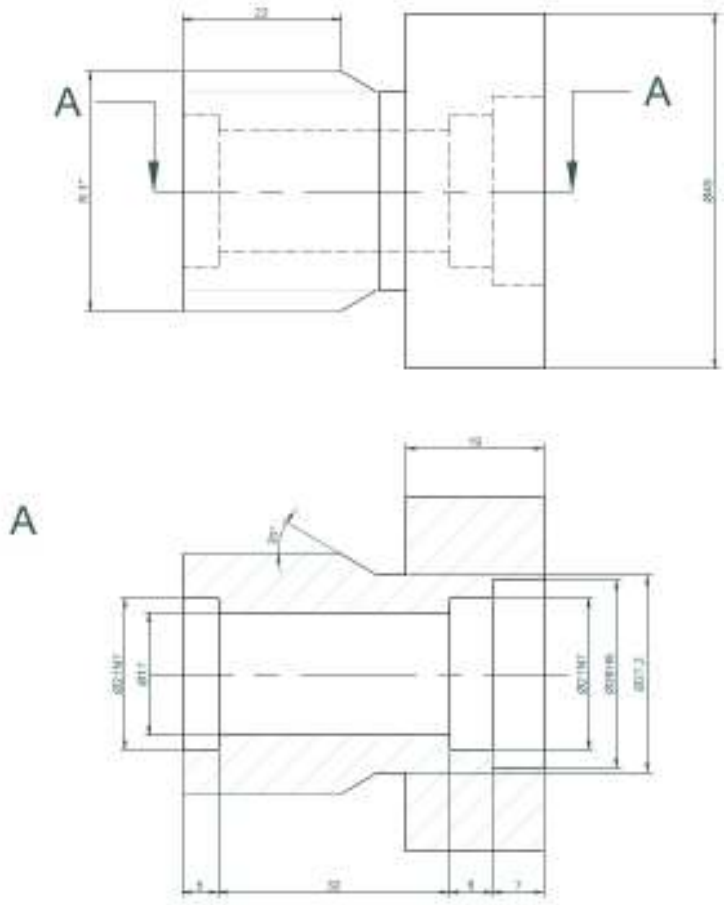

Figure 2.5: Technical drawing of penetration

The outside of the shaft penetration is threaded with 1"BSP external threads. A female 1"BSP socket was welded to the ROV hull. 577 Loctite thread sealant was applied to the external threads and screwed in the socket. Figure 2.6 shows the finished machined parts.

Figure 2.6: Machined parts of shaft system

Pressure testing

After finished welding and mounting of every component that was meant resisting water from entering, the ROV was put through two tests of waterproofing before any electronics were installed. The first test was done in a towing tank. A hose was connected to one of the cable penetration's sockets. The ROV body was submerged underwater while an internal air pressure was created by blowing into the hose, and checking for bubbles. The second test was done in the sea. A steel block was tied to the ROV body and sunk 20m. After 10 minutes, the ROV body was put back ashore and opened to see if water had entered.

Buoyancy calculations and measurements

The mass of the ROV body, camera arrangement, echo sounder, wings, and side plates was measured separately. The ROV body had all its internal components installed at the time of the measurements. An Excel spreadsheet was created for the calculations. Figure 2.7 shows the mass measurements.

	Mass measurements		
	ROV body	26,3	kg
2	Lights with clamping	0,6	kg
	Camera arrangement	1,4	kg
	Echo sounder	0,1	kg
	Sum of components added later		kg
2	Side plates	2,6	kg
2	Wings	1,9	kg
	ROV_{tot}	32,8	kg

Figure 2.7: Mass measurements

The net freshwater buoyancy was measured in the towing tank using a digital scale attached to the ceiling, and a rope passing through two pulleys in the bottom of the tank. The displaced volume and seawater buoyancy were calculated using the equation $\rho = \frac{m}{volume}$. The buoyancy calculations are shown in figure 2.8

	Net buoyancy measurements (fresh water)		
	ROV body, lights, camera, echo sounder	133,4	N
2	Side plates	-1,9	N
2	Wings	1,0	N
	ROV_{tot}	132,5	N
	Calculated volume of displaced fluid		
	ROV body, lights, camera, echo sounder	0,042	m^3
2	Side plates	0,0024	m^3
2	Wings	0,0020	m^3
	ROV_{tot}	0,046	m^3
	Calculatet net sea water buoyancy		
	ROV body, lights, camera, echo sounder	144,5	N
2	Side plates	-1,2	N
2	Wings	1,5	N
	Sum of components added later	0	N
	ROV_{tot}	144,8	N

Figure 2.8: Buoyancy calculations

2.3.1 Transmission introduction

The motor extends and retracts a shaft linearly. A geared system was chosen to rotate the wing shafts.

2.3.2 Transmission selection

In the previous version of the ROV's transmission system, an aluminium arm was extended from the wing shaft's centre. A hollow round steel bulb was attached to the motor's shaft. The steel bulb was rotating on a steel ball bolted to the aluminium arm. The motor was attached to door hinges that adjusted the motor's angle as the wing shaft was rotating. This method of transmitting linear to rotating motion is effective, however, the parts used were not rigid and had poor precision. To improve the construction, one would need to mount the motor on a shaft somehow rotating on a single ball bearing below the centre of the motor, or between two ball bearings. The motor shaft's attachment to the arm extended from the wing shaft would need to rotate between two ball bearings or a shaft trough one bearing at the arms centre to avoid a high bending moment. This solution would require time-consuming and high precision machining. The method is explained in figure 2.9

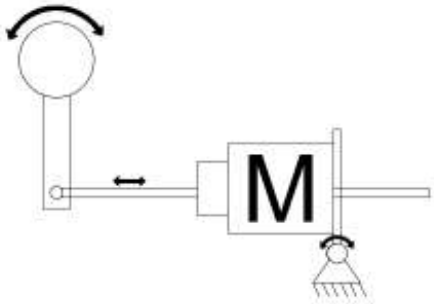

Figure 2.9: Method of transmission

We chose gears for this ROV version's power transmission system. The force from the motor shaft transmits torque on the wing shaft gear with a gear rack. The gear rack is moving in dovetails. The friction in the dovetail solution has a negative impact on the power transmission efficiency, see section 2.3.3. However with this solution the motor is fixed, it's simple to adjust the torque ratio whilst keeping a rigid construction, and the construction is easily 3D printed. This method is explained in 2.10

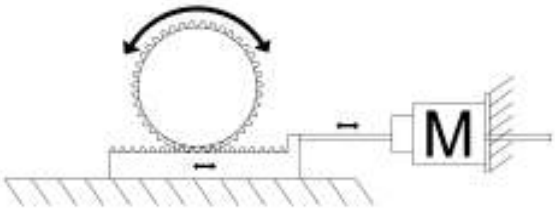

Figure 2.10: Chosen method of transmission

2.3.3 Building and solutions

Three different spur gears were modelled in Siemens NX to make the angular velocities of $10°/s$, $7.5°/s$, and $5°/s$ in relation to the shaft speed of 3.75mm/s. The gears were 3D-printed in PLA-plastic with a module one tooth profile. Shorter teeth are subjected to a smaller bending moment which is especially important in 3D-printed gears due to the weaker material and that it's built up of many strings of melted plastic rather than a solid casting. A silicone mould was made from every gear. A two-component polyurethane was used to cast stronger gears. Every gear tooth was cast successfully. However, the gear rack's dovetail was not sharp enough to travel as friction-less as preferred. It was decided to use 3D-printed gear racks and cast gears. To manufacture gear racks in the stronger plastic material, we would have to oversize the mould, and machine down a better fit in a mill.

The motor and gear rack is mounted on an aluminium flat bar that travels along two stainless M10 threaded rods. When mounting a gear on the wing shaft, one

would adjust the height of the flat bar so that the two gears mesh. The flat bar is then locked with two nuts on each threaded rod.

Transmission calculations

The motor's power is according to the datasheet provided from supplier, rated to 10W. However, this is electrical power. The shafts travelled linearly at 3.75mm/s, with a force of 65N, see figure 2.18. Making the shaft's mechanical power when we did the majority of tests as described in equation 2.1.

$$P = F \cdot v = 65N \cdot 0.00375m/s = 0.243W \tag{2.1}$$

Ball bearings mechanical efficiency is set to $\eta_{bb} = 99\%$. If three ball bearings are used to improve the method used in the previous ROV, described in 2.3.2, the power transmitted to the wing shaft is calculated in equation 2.2.

$$P_{bb} = P \cdot \eta_{bb}^3 = 0.243W \cdot 0,99^3 = 0.235W \tag{2.2}$$

We can compare the ball bearing system and the geared system with simple calculations. The magnitude of the sliding friction force on the 3D-printed gear rack's movement on another 3D-printed surface is dependent on the magnitude of the force pushing them together. This force depends on the mounting described in 2.3.3. Ideally, the mounting results in gear teeth mesh with no additional force pushing the to parts against each other.

We can find the theoretical force needed to push the two 3D-printed surfaces together so that the friction force alone accounts for the same power loss as the three bearing example above. This force will of course also impact the rolling friction of the gear teeth, and lower the gear's efficiency. A free body diagram of the system is shown in figur 2.11

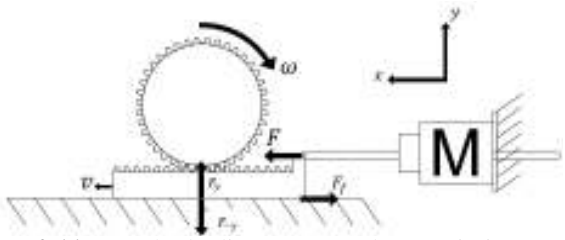

Figure 2.11: Free body diagram geared transmission system

The sliding friction force is found by calculating $F_f = \mu_p \cdot F_y$. The coefficient of sliding friction between two plastic parts is set to $\mu_p = 0,3$, and F_y is the pushing

force normal to the two surfaces. The loss in force magnitude on the three bearing system is found by the equation 2.3.

$$F_{lost} = F - \frac{P_{bb}}{v} = 65N - \frac{0,23W}{0,00375m/s} = 3,7N \tag{2.3}$$

The needed F_y force to result in the friction force F_f only between the sliding part of this magnitude is found by the equation 2.4.

$$F_y = \frac{F_f}{\mu_p} = \frac{3,7N}{0,3} = 12,3N \tag{2.4}$$

If this force is halved to approximately include the gears rolling friction we get 6.3N. A force with this magnitude will not be subjected on the gears if mounted properly. A more reasonably force to continue the calculation with is $F_y = 3N$. The efficiency on our non lubricated plastic gears are set to $\eta_g = 97\%$. The power transmitted to the wing shaft is found by the equation 2.5.

$$P_g = (F - \mu_p \cdot F_y) \cdot v \cdot \eta_g = (65N - 0.3 \cdot 3N) \cdot 0.00375m/s \cdot 0.97 = 0.23W \tag{2.5}$$

Adding the mechanical efficiency for the two ball bearings on the wing shaft in equation 2.6.

$$P_{ws} = P_g \cdot \eta_{bb}^2 = 0,23W \cdot 0,99^2 = 0.225W \tag{2.6}$$

The linear velocity $v = 0.00375m/s$ on the gear rack is the peripheral velocity on the wing shafts gear. This gear has the pitch diameter $D_p = 68mm$. The angular velocity of the wing shaft is found by the equation 2.7.

$$\omega = \frac{v}{(\frac{D_p}{2})} = \frac{0.00375m/s}{(\frac{0.068m}{2})} = 0.1103s^{-1} \tag{2.7}$$

The low rpm of the shaft makes it impractical to find the power lost in the shaft seal friction on graphs provided by the supplier. We can use a simple calculation to approximate it. The young's modulus of nitrile butadiene rubber (NBR) $E = 1.3MPa$. The shaft seal's inner diameter is 9mm. It was pressed on to a 10mm shaft, making $\Delta L = -1mm$, negative due to compression. The width of the contact surface is 2mm. We can now find the force exerted on to the shaft by the seal by solving the equation 2.8.

$$F_{seal} = \frac{E \cdot A \cdot \Delta L}{L_0} = \frac{1.3 \cdot 10^6 Pa \cdot (\pi \cdot 0.01m \cdot 0.002m) \cdot (-0.001m)}{0.01m} = -8N \tag{2.8}$$

The resulting normal force N is used to solve for the sliding friction force F_{fs}. The sliding friction coefficient in NBR on steel is found in figure 2.12.

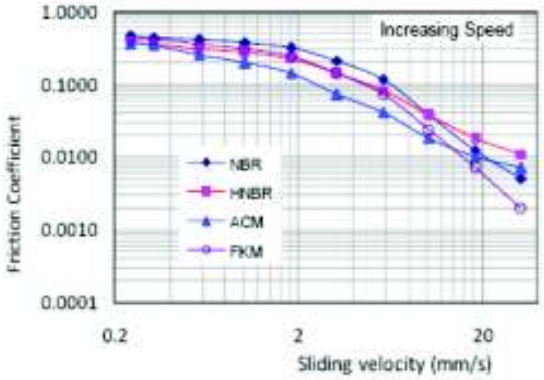

Figure 2.12: Sliding friction coefficient NBR on steel[1]

With the angular velocity and the shaft's diameter, we find the shaft's peripheral velocity at the sealing point with equation 2.9.

$$v_s = \omega \cdot \frac{d}{2} = 0.1103s^{-1} \cdot \frac{10mm}{2} = 0.6mm/s \tag{2.9}$$

Giving us a sliding friction coefficient $\mu_{NBR} = 0.6$. The shaft seal friction force is calculated in equation 2.10.

$$F_{fs} = \mu_{NBR} \cdot N = 0.6 \cdot 8N = 4.8N \tag{2.10}$$

The shaft's torque τ_{shaft} after the two shaft bearings are found by the equation 2.11.

$$\tau_w = \frac{P_{ws}}{\omega} = \frac{0.225W}{0.1103s^{-1}} = 2.04Nm \tag{2.11}$$

The force F_{shaft} where the shaft is sliding at the seal is calculated in equation 2.12.

$$F_{shaft} = \frac{\tau_{shaft}}{d/2} = \frac{2.04Nm}{0.01m/2} = 408N \tag{2.12}$$

The torque subjected to the wings can now be calculated with equation 2.13.

$$\tau_{wing} = (F_{shaft} - F_{fs}) \cdot \frac{d}{2} = (408N - 4.8N) \cdot \frac{0.01m}{2} = 2.02Nm \quad (2.13)$$

Making the power as shown in equation 2.14.

$$P_{wing} = \tau_{wing} \cdot \omega = 2.02Nm \cdot 0.1103s^{-1} = 0.222W \quad (2.14)$$

The transmission system's mechanical efficiency is calculated in equation 2.15.

$$\eta_m = \frac{P_{wing}}{P} \cdot 100\% = \frac{0.222W}{0.244W} \cdot 100\% = 91\% \quad (2.15)$$

2.3.4 Wing introduction

The wings works as the actuators controlling the ROV and the design is crucial for the ability to control the ROV as intended.

2.3.5 Wing profile selection

When applying the lift equation ($L = \frac{\rho}{2} C_L v^2 A$) based on Bernoulli's principle on potential wing shapes suited for the ROV, it was clear that the lift forces in a fluid like sea water was far greater than any other force the wings needed to compensate for. Even with a relatively small wet area, the lift force would have a substantial impact on the ROV's movement. And when not knowing the lift forces created by the ROV body, we focused the wing design to minimize additional turbulence's, simple mount/dismount and strong enough to withstand a lot of handling

3D-printing is a good way to produce complex shapes, but 3D prints buoyancy are high. It was decided to print the shape and fill the internal volume with polyurethane to make them more neutral in the water.

It was reasonable to test a symmetric wing profile first. This profile allows for no generated lift force when there's no angle between the wing and the direction of the water flow. The size was determined based on the largest we could fit in a 3D-printer. The plan was to make several in different sizes, but other tasks was prioritized.

2.3.6 Building and solutions

The wings was 3D modeled in Siemens NX. They were 3D-printed shelled with a 5mm wall thickness with PLA as material. Two M6 threaded rods were placed

inside 3D-printed plates with pilot holes with the same centre distance as the wing flanges bolt holes. The rods were then placed inside the wings, and a two component casting polyurethane was poured in. 3D-prints in PLA attracts water, so the wings was primed and painted.

2.3.7 Wing calculations

The forces acting on the wings whilst the ROV is operating should not create a torque that surpasses the torque subjected on them by the transmission system $\tau_{wing} = 2.02Nm$ within the range of desired wing angles. The wings weight in seawater is negligible. The dimensions of the wings are given in mm in figure 2.13.

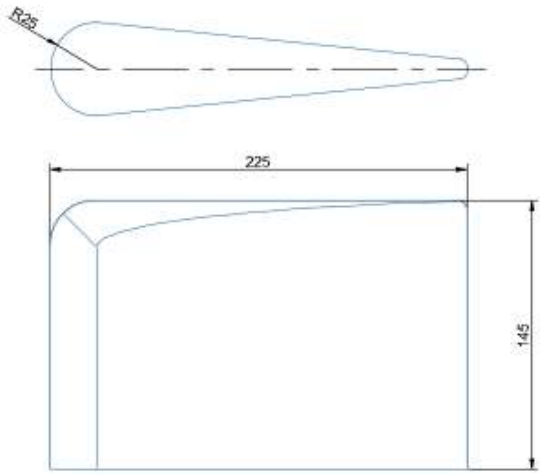

Figure 2.13: Wing currently used on ROV

The wing's lift force attacks from the centre of volume. To simplify our centre of volume calculation, we will only calculate the hydrofoil cross-section and assume constant thickness.

The wing is divided into three areas, two half circles and a trapezoid. Finding the centre of volume of each area was done graphically in Autocad. Figures 2.14 and 2.15 shows how.

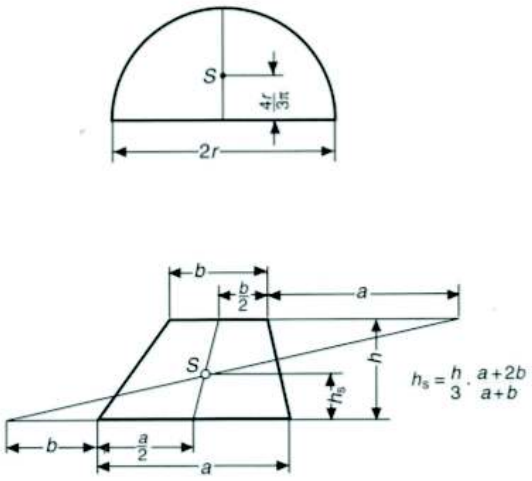

Figure 2.14: Trapezoidal and half circle's center of mass [2]

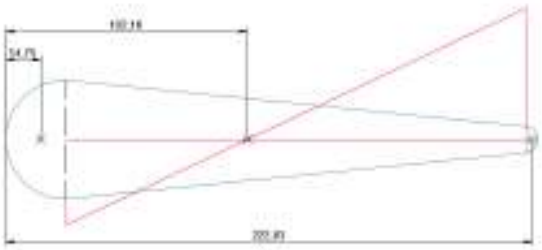

Figure 2.15: Graphic solution in Autocad

The combined centre of volume is then found with equation 2.16.

$$\bar{x} = \frac{\sum A_i \cdot x_i}{\sum A_i} = \frac{\frac{\pi \cdot D^2}{8} \cdot x_1 + \frac{a+b}{2} \cdot h \cdot x_2 + \frac{\pi \cdot d^2}{8} \cdot x_3}{\frac{\pi \cdot D^2}{8} + \frac{a+b}{2} \cdot h + \frac{\pi \cdot d^2}{8}} \tag{2.16}$$

$$= \frac{\frac{\pi \cdot 50^2 mm}{8} \cdot 14.75mm + \frac{11mm+50mm}{2} \cdot 150mm \cdot 102mm + \frac{\pi \cdot 11^2 mm}{8} \cdot 223mm}{\frac{\pi \cdot 50^2 mm}{8} + \frac{11mm+50mm}{2} \cdot 150mm + \frac{\pi \cdot 11^2 mm}{8}} \approx 88mm$$

A simplified method of calculating the drag force the wings are subjected to is to use the projected area the wings have in relations to the direction of the water flow. Wings tested in wind tunnels that are similar to the shape of the wings currently on the ROV, show that the lift coefficient is peaking around the wing angle of $15°$ in relation to fluid flow [**?**]. This should ideally be the maximum wing angle. When rotating the wing $15°$, the drag force can be placed on the projected square's centre.

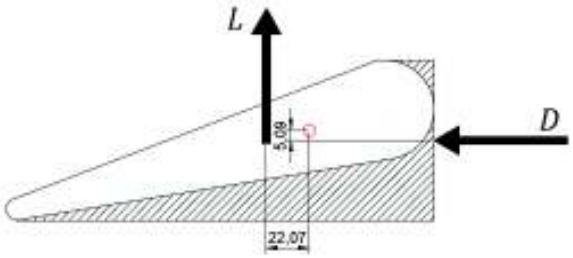

Figure 2.16: Drag and lift force placed. The red circle is the shaft

The drag coefficient C_D is set to 0.01, and the lift coefficient C_L is found using the equation shown in figure 2.17.

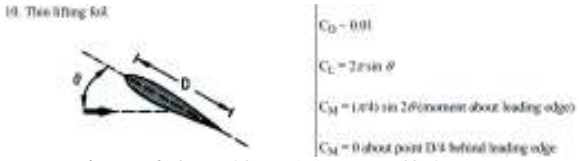

Figure 2.17: Lift and drag coefficient [3]

The maximum operable speed was 5.5 knots = 2.8m/s. The wing's area was calculated from the Siemens NX 3D-model to be $0.075m^2$. Calculating the Lift force F_L and drag force F_D.

$$F_L = \frac{\rho_{seawater}}{2} \cdot C_L \cdot v_{ROV}^2 \cdot A_{wing} = \frac{1025kg/m^3}{2} \cdot 1.6 \cdot 2.8^2 m/s \cdot 0.075m^3 = 482N \tag{2.17}$$

$$F_D = \frac{\rho_{seawater}}{2} \cdot C_D \cdot v_{ROV}^2 \cdot A_{p15^\circ} = \frac{1025kg/m^3}{2} \cdot 0.01 \cdot 2.8^2 m/s \cdot (0.145m \cdot 0.081m) = 0.5N \tag{2.18}$$

The torque caused by these two forces are acting on the wing shaft in the same direction and is defined negatively compared to the wing shaft torque.

$$\sum \tau = \tau_{wing} - \tau_{F_D} - \tau_{F_L} = 2.02Nm - 0.005m \cdot 0.5N - 0.022m \cdot 482N \tag{2.19}$$

$$= 2.02Nm - 0.0025Nm - 10.6Nm = -8.6Nm$$

This shows that at some point while turning the wings, the motors will stall. The maximum wing angle can be calculated. Ignoring the drag force due to the short moment arm. The shaft's torque direction is defined as positive.

$$\sum \tau = 0 \tag{2.20}$$

$$\tau_{wing} - 0.022m \cdot (\frac{\rho_{seawater}}{2} \cdot 2\pi \cdot sin(\theta) \cdot v_{ROV}^2 \cdot A_{wing}) = 0$$

$$\theta = sin^{-1}(-\frac{\tau_{wing} \cdot 2}{0.022m \cdot \rho_{seawater} \cdot 2\pi \cdot v_{ROV}^2 \cdot A_{wing}})$$

$$= sin^{-1}(-\frac{2.02Nm \cdot 2}{0.022m \cdot 1025kg/m^3 \cdot 2\pi \cdot 2.8^2 m/s \cdot 0.075m^2}) = -2.8^\circ$$

Using the same equation shows that by reducing the velocity to 1.5m/s=2.9knots, the maximum wing angle increases to ten degrees.

2.4 Introduction hardware

For the ROV to operate as intended, it needs hardware devices to collect and handle data, perform logic and control actuators. Most of the hardware used in this project comes from the previous ROV, as the new ROV is intended to perform the same set of tasks.

2.5 Hardware selection and previous solution

2.5.1 Raspberry Pi

The raspberry pi is a small computer operating on a Linux operating system. The operating system provides the user to set up and include the program language they see fit. The Pi comes with a range of inputs and outputs, as well as RJ45 and USB connections. It is well suited for the ROV project as it is small and fast enough to carry out the relatively simple tasks. There were two Pi's from the previous project, one working as the main computer, communicating with all units in the ROV, including the GUI. The PID controller was also implemented in the code. The other PI was placed in the camera housing, handling the camera, servo motors for controlling the camera and a depth sensor.

2.5.2 Arduino

Arduino is an open-source microcontroller based on c++. It is well suited to handle I/O, low-level logic and math. There were three Arduinos in the previous ROV. One Arduino nano for controlling internal led light, and two Arduino Uno. One Uno was used for controlling the stepper motors, while the other handled the echo sounder.

2.5.3 Structural changes hardware

We decided to remove the internal led lights as they have no purpose in an aluminium body. We made two more structural changes with the Arduinos. The first change was to move the depth sensor from the camera Pi to the Arduino handling the echo sounder. The other change we made was to move the PID controller to the Arduino moving the steppers. We discussed if this would make the steppers move slower, but we figured it would run at the same speed as the steppers need about 3ms between the pulses. These changes are made to separate the tasks of each controller, providing a more obvious structure.

2.5.4 PCB board

A previous group built the PCB board to convert the input voltage to 5V and 12V. One of the 12V DC/DC converters was defective, so it was replaced.

2.5.5 Stepper motor RS PRO 42dbl10

The previous ROV group changed from linear actuators with brushed DC motors to a linear stepper. The reason was that the actuators initially mounted was damaged due to the oil in the actuator boxes. The stepper motor is well suited for the ROV and can achieve high torque at low speed. The force/speed ratio for the 42DBL10 stepper is described in figure 2.18.

Figure 2.18: Force/speed stepper motor

2.5.6 Pololu md20b stepper controller

We kept the stepper controllers that were being used by the previous group. When testing the stepper controllers, we discovered that one of them was defective, so we had to replace it. The functions applied are stepping the motors and changing direction.

2.5.7 Camera

As there were some problems with the picture quality, we decided to try a new camera. A low light USB camera from blue robotics was chosen because of its ability to get good picture/video in low light (deep sea). It achieves a better low light image by using a large camera sensor and a low pixel count. Then each physical pixel size is large to get maximum light sensitivity. Since the previous Towed-ROV used a Raspberry pi camera and not USB, a bit of rework in the code to capture the image was necessary. The old code used library specifically for RPI camera, this is now changed to Open-CV. The camera was mounted on a small servo to adjust for the change in pitch on the ROV.

2.5.8 Depth sensor

For measuring the depth of the ROV, the same MS5837-30BA (Figure 2.19) pressure sensor implemented in the previous ROV is used. The MS5837-30BA has a working area between 0-30 bar (converted to meters), with a resolution of 200 millibars. For communication between microcontroller and sensor I2C is used. Additionally, the sensor comes with a temperature sensor, with an accuracy of $\pm 1°C$, limited to -20 to 85°C. One of the main reason for choosing this sensor was its simplicity as well as a physical threaded section, which made it easy to mount to the ROV body, and the risk for leakage is minimal. However, it is important to keep the wiring as short as possible since the I2C has a limited transmitting distance

Figure 2.19: MS5837-30BA

2.5.9 Echo sounder

The echo sounder mounted on the previous ROV was not certified for more than 3 meters of depth. For that reason, we had to find an echo sounder that was better suited. We ended up with blue robotics ping sonar (Figure 2.20), as it was cheap and able to handle up to 30 bars. The ping sonar is a single-beam echo sounder, with a measurement range of 30 meters and a beamwidth of 30 degrees. It uses a transducer frequency of 115 kHz, which is different from most other echo

sounders, this eliminates potential interference from an echo sounder mounted on the boat [6].

Figure 2.20: Ping sonar

However, as the blue robotics ROV operates at a low speed, with not much of a pitch angle, we need to make some tests to see if the ping sonar is accurate enough.

2.5.10 Magnetic proximity sensor

These are the same as the previous version of Towed-ROV used to reset the stepper motor. There are two proximity sensor, one for each stepper motor, both connected to Arduino Uno.

2.5.11 Water detection

The previous ROV had leak sensors to detect leakage in the camera housing. The sensors are moved to the main body as it is not filled with oil. Both sensors are mounted as close to the flange (lowest point) as possible on opposite sides.

2.5.12 IMU

In the previous Towed-ROV, a 9Dof Razor IMU M0 (Figure 2.21) has been used to monitor the pitch, roll and heading of the Towed-ROV. The IMU comes with a SAMD21 microprocessor. We made a slight adjustment to the existing code, removing some of the measurements that are not being used.

Figure 2.21: IMU

2.5.13 Humidity and temperature sensor - HIH6130

The HIH6130 sensor (Figure 2.22) from previous Towed-ROV, was still kept for to monitor the humidity in the Towed-ROV. Because the amount of heat two Raspberry Pis and two stepper motors can produce, the humidity may get to a level that can damage the electronics if the conditions are right. The HIH6130 is connected to the camera RPI with I2C communication.

Figure 2.22: HIH6130

2.5.14 Electronics mounting and wiring

The electronics inside the Towed-ROV was mounted on an acrylic plate (split to 4 parts), this is done to remove and do changes on the electronics easily. Also, it's a protection against the electrical conductive aluminium body (Figure 2.23).

Figure 2.23: Electronics mounting

Wiring schematic can be found in the appendix 3.5.1

2.6 Sensor software

The IMU, depth sensor and echo sounder all comes with a library developed by the respective producers. Both the IMU and echo sounder comes with filters, while we implemented a kalman filter for the depth sensor.

IMU

The IMU runs on the Razor AHRS firmware, including a DLC/kalman filter.

Echo sounder

Blue robotics have developed a library for their Ping sonar. Converting the data to depth and accuracy. There is a filtering algorithm included.

Depth

Blue robotics has developed a library for the depth sensor. However, as there is some noise in the signal, a Kalman filter was implemented in the Arduino. The way a Kalman filter work is to first estimates a "priori" estimated state by using an initial educated guess on what the initial condition would be. It also estimates the "priori" error covariance. Then the Kalman gain is calculated. Kalman gain is a scalar between 0 and 1. If the Kalman gain is close to one, the measured value will count more than the estimated value when calculating the "posteriori" estimate which is the output and vice versa for a gain close to zero. Finally, before the filter repeats, it updates the error covariance. The "posteriori" estimate multiplied with the A matrix will become the new "priori" estimate. The loop is described in figure 2.24.

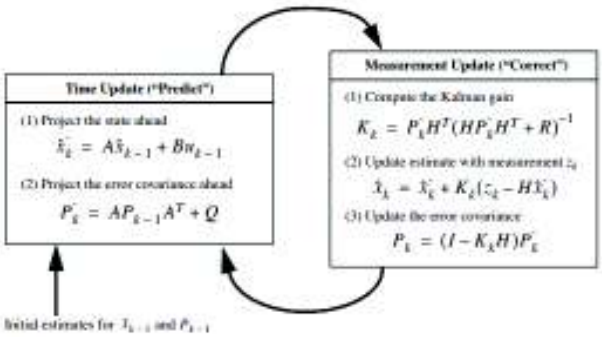

Figure 2.24: Kalman Filter[4]

The kalman library is written by Denys Sene, and can be installed directly from the Arduino IDE.

2.7 Control system introduction

For a dynamic system to operate as intended a controller is introduced. The purpose of the controller is to control actuators based on changes in a process. For the ROV project, the only actuators are the wings. The depth of the ROV and trim angle can be adjusted by changing the angles.

2.8 Control system selection

An ROV operating in the ocean is a highly nonlinear system with potential many disturbances. The complexity of the system makes it difficult to calculate a mathematical model, as modern control theory relays on. A more practical solution is to use PID controllers, that calculates the output based on changes in the process, without any knowledge of the system. Instead the PID controller relies on an operator tuning the parameters. When applying a linear controller to a nonlinear system, the controller would most likely be more ideal in a certain range.

2.8.1 Selection PID algorithm

The PID equation can be separated in to three different types with different characteristics. They are often described as type A, B and C [**?**].

PID type A

Type A controller is expressed with equation 2.21.

$$U(t) = K_p e(t) + K_i \int_0^t e(t')dt' + K_d \frac{de(t)}{dt} \tag{2.21}$$

Where U(t) is the output and e(t) is the error between reference and measured value. The type A controller can be ideal for regulating a system with constant reference. The problem with the type A controller is when the reference changes, this will lead to a spike in the control output.

PID type B

Type A controller is expressed with equation 2.23.

$$U(t) = K_p e(t) + K_i \int_0^t e(t')dt' - K_d \frac{dy(t)}{dt} \tag{2.22}$$

Where y is the measured state. By changing the D term to react on change of measurement, the spike from a change in reference is avoided. For the ROV where the angles of the wings are quite slow due to the speed of the stepper motors this might not make a big difference. However as we are not yet certain about how

much a small change in angle will impact the change of depth we believe the type B controller is better suited.

PID type C

Type C controller is expressed with equation 2.23.

$$U(t) = -K_p y(t) + K_i \int_0^t e(t')dt' - K_d \frac{dy(t)}{dt} \tag{2.23}$$

In a type C controller the P term is now restricting the output and will work together with the D term. Meaning that an increase in the P parameter will make the system slower. However, any kick from change in setpoint is avoided.

Conclusion on PID type

For the ROV to follow the sea floor, the set point will change continually depending on the sea floor. For this reason we believe PID type A will provide disturbance in form of a derivative kick. We believe the system will respond best if it is proportional on error for quick response if an obstacle is observed. For these reasons we have decided to go for PID type B for depth control. The trim PID will work as an regulator with a constant reference so the derivative kick will not appear. However, as we see no reason for not using a PID type B we have chose to use the same PID for trim.

Integral wind up

For systems with actuator limits the integral term can lead to some problems if not handled correctly. If the controller only constrains the output of the entire equation, the I term can by time increase far beyond bounds. Especially in slower systems can this be a crucial problem. There are several ways to handle windup, there can be a feedback loop measuring the actuators input and output. A cheaper and easier method is constraining the integral value.

Choosing PID library

There are several PID librarys for Arduino. When selecting the controller we had some requirements.

- Bumpless on/off
- Able to change parameters on the go
- Integral anti windup
- PID type B

All the requirements listed is handled in Arduino PID by Brett Beauregard. There were still two issues, the first was that the integral limit is set to be the same as

the output limit, so we added a function to set a separete integral limit. The other issue was that when the integral gain is set to zero, the sum of the integral keeps the same value, denying the previous integral contribution to be canceled out. This was sorted by setting the integral sum to zero when ki is set to zero.

2.9 Control implementation

figure 2.25 describes the flow of the Arduino program for controlling the wings. Data sent from the ROV computer is a string with one seperator, the first part is a header, while the second part is a value. The program operates in three different modes. Manual, auto depth and auto sea floor. Manual mode sets a wing angle from a GUI input, while the auto modes are explained in 2.9.1.

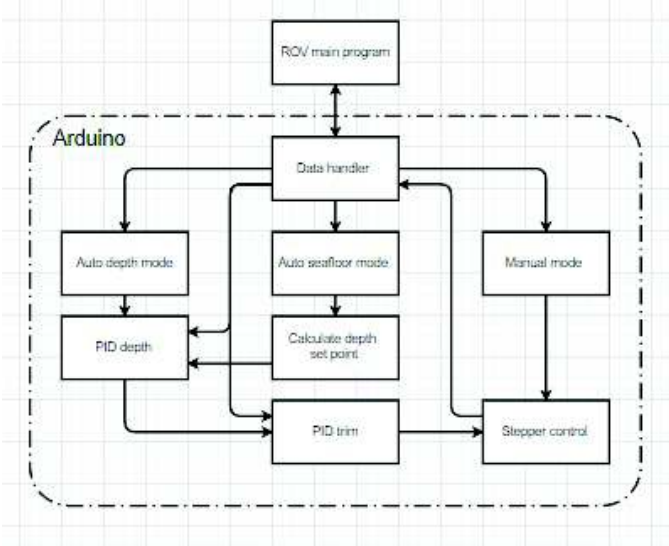

Figure 2.25: Arduino wing control

2.9.1 Control system

To control the ROV as intended we need two PID controllers. One for depth and another for trim. For depth control the operator will manually set the depth set point, while for sea floor control, the depth set point will be automatically set based on the measurements of the echo sounders. Figure 2.26 describes the control system.

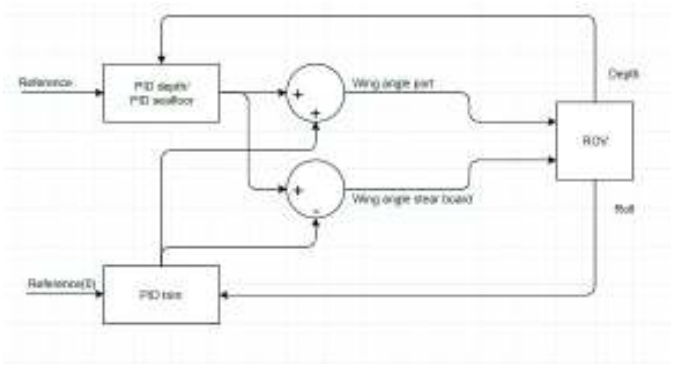

Figure 2.26: PID diagram

2.9.2 Controlling the motors

There was a code from the previous group for moving the steppers. This code worked quite well but relied on several delays to prevent the pulses from being to rapid. Another problem was that the steppers could not be moved individually, refusing the ROV to perform trim for stabilisation.

Since the Arduino controlling the motors had no other tasks, and the motors always moved in the same direction together. The delay was not a big issue. However, when the Arduino has to perform several tasks, these delays will stop the program. Controlling the steppers individually, they will at some point have to move one at a time, if there is a delay of 4ms between each puls the loop would get relatively slow. These delays stops the entire program, denying any functions to be carried out. To prevent this, we introduced timers, that checked if a certain time had passed. Another solution could be to use a state machine with every possible combination of steps.

2.9.3 Tuning

When tuning a PID it is important to have some thoughts on how a change in a parameter will affect the system. One should also have an idea how a certain value will contribute to the output in different scenarios. However, before tuning the PID it is crucial to know how the system reacts to the system inputs. This can be done by controlling the wings manually.

The controller were tuned with a constant speed on the boat, approximately 3.5 knots. The ROV stabilized with wing position 0°at about 11 meters depth. To see what range the ROV were physical able to perform, the ROV were controlled manually, the range in depth were 7-13 meters of depth.

The objective is to get a system with a fast transient response and a stable steady state response. The overshoot should be held to a minimum. These characteristics

should be good for sea floor tracking, as the transient response are necessary to avoid obstacles, and the stable steady state would make the picture quality better.

The result of the tuning process is described in figure 3.10 and table 3.1.

2.10 GUI introduction

From earlier iteration of the Towed ROV a GUI as already established.

2.11 GUI selection

There are three options when selection GUI, build a new one or use existing GUI.

2.11.1 Create new GUI

With the reason that the current GUI is not optimal. Building a new GUI can save time in the long run and give better functionality.

2.11.2 Use existing GUI

The existing GUI has most of the feature that is needed for this project already. Short term this saves the group a lot of time in a project with already limited time. On the other hand, the code whole code needs a refactor.

2.12 GUI implementation

2.12.1 Use existing GUI

The group decided to use the existing GUI with minimal changes, which saves time and also the group can collect information about the existing GUI, what is practical and not. Some refactoring of the code was done when implementing new changes. The changes made to the existing GUI:

- Added option to set PID parameter for trim.
- Change manual control to set manual wing position in degrees and not step-position
- Display wing position in degrees.
- Added target distance(setpoint) and ROV echo-sounder to existing live plot
- Added new live plot for pitch and roll
- Fixed some logic when changing mode
- Added pitch offset to adjust the angle of the camera servo

2.13 Communication introduction

Most of the software used for communication is implemented from the previous ROV. However, some changes had to be made, as there were some restructuring of components and logic. The communication setup is described in figure **??**

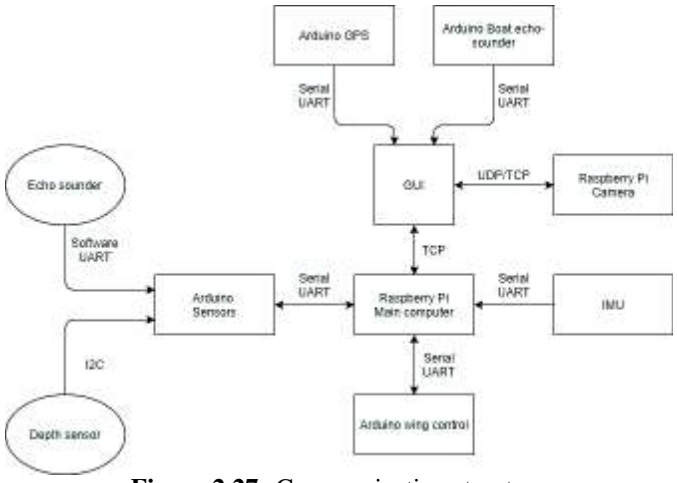

Figure 2.27: Communication structure

2.14 Communication implementation

2.14.1 Computer(Gui) to Raspberry pi

The communication between Gui and the Raspberry Pis was already established on the precious ROV. UDP sockets are set up for transmitting the video stream, as it is a lot faster than TCP, and some lost packets will not affect the quality of the stream. While the rest of the data is mostly commands, that requires far fewer packets, but all of them must arrive for the message to make sense. These requirements make TCP well suited, as TCP is connection-oriented and comes with error recovery.

2.14.2 Raspberry pi to Arduino and IMU

To communicate with the two Arduinos and the IMU, serial UART is used. This is the same as the previous ROV. In this project, the PID controller was moved from RPi to an Arduino, this meant that the Arduino needed to get sensor value from RPi, leading to more communication between the Pi and Arduino. The previous version used Serial.readString(), to read the message sent from the RPI. However this was noticed to be slow(the Serial.readString() could not keep up with the incoming data). Implementing Serial.read() is a better solution, as it takes one byte from the buffer for each loop. We used an end marker to tell when all of the data is received. There have been no issues sending complete strings.

2.14.3 Sensors

Depth sensor(MS5837): The depth sensor is integrated with i2c communication. When testing on the labs with an external power supply, it worked fine. However, when we connected the batteries to power the ROV, the sensor wouldn't initialise. After consulting with Ottar Osen, we tried moving the Arduino closer to the sensor since I2C was originally built for communication on an integrated circuit. Further, we slowed down the clock speed of the I2C. With a combination of the two test mention above the sensor would communicate. The root of the I2C problem was probably increased interference when the batteries were connected. We added aluminium tape around the sensor wire as well as the input power, for shielding.

Echosounder(Ping sonar) Software UART is used to communicate with the Ping sonar. This is implemented using the Arduino library "SoftwareSerial". Software UART is a software replication of the Serial UART allowing UART communication on hardware not supporting Serial UART. Due to the echo sounder is connected to an Arduino Uno with one hardware serial UART(used for communication to Raspberry Pi), software UART is implemented. Software UART is possible using "Bit-baning"(creating a series of pulses in software rather than in hardware). Bit-banging is more processor consuming, and not as precise as serial UART. https://learn.sparkfun.com/tutorials/serial-communication/uarts

2.15 Simulation introduction

The goal for the simulation was to make a simulation that could tune the controller parameters of the PID, such that the time spent manually tuning it would be decreased to a minimum. Also, the possibility to design and test more advance controller and tune controllers with a genetic algorithm was an objective.

2.16 Simulation selection

2.16.1 Mathematical model

It's hard to get a precise mathematical model, but possible. However, it will take a lot of time and effort to make it. If succeeded, creating new controllers and tune them will be easier and quicker.

2.16.2 AGX Dynamics

AGX Dynamics is a professional modular physics engine for the simulator. Where you can import your model and in our case, use pre-built hydrodynamics (in AGX) to be able to simulate the Towed-ROV behaviour in water. AGX also has a key advantage in the visualisation of the simulation, this is valuable when it does not

behave as intended. However, the advance dynamics and visualisation will be restricted by the hardware of the pc running the simulation[7].

2.17 Simulation implementation

2.17.1 AGX Dynamics

Since our system is of great complexity, finding the transfer function of our model mathematical, is difficult and time-consuming. Therefore a simulation in AGX Dynamics was chosen.

Towed-Rov

The model was split into three parts, right and left-wing as well as the main body. Since the 3d-model is to detailed for our computers hardware, the model had to be simplified, first by removing detailed part with the least effect on the hydrodynamics of the Towed-ROV, such as nuts, bolts, threaded rods and lights. The model was imported as OBJ file, a geometric file type using many small triangles put together to represent the model. By using this type of file, we could make the model less detailed by reducing the amount of triangle used to represent the model. This made the simulation smoother, but the hydrodynamics of the model was not precise as original. This process was also done for the wings.

Since mass is a product of density and volume (equation 2.24) setting the correct mass and density is hard when AGX doesn't care about units when importing the OBJ-file.

$$\rho = Mass/Volume \tag{2.24}$$

Therefore the volume of the ROV has to be scaled correctly to get the correct density when setting the mass. If one of the three factors is not correct, the simulation will be not precise. One way to get the correct mass and density is by testing different scaling of the ROV.

By creating an AGX assembly, the Towed-ROV was put together by manual setting the position of the wings onto the ROV body. To rotate the wings around a fixed point on the ROV body, a constrain (hinge) was made for each wing and restricted to only rotate in around the y-axis.

Towed-Rov controller

To control the angle of the wing of the Towed-ROV an output is needed to be set to the constrain. This output needs to be mapped for each wing since they are not positioned on the same point, here we also restrict the output angle on wings to the same as the actual model $\pm 45°$.

Boat

To tow the ROV, a boat was created by using the "Ship in water" example code from AGX Dynamics. Adjustment to the code was made to be suited for our simulation. Mainly scaling of the physical size of the boat but also forces acting on the boat. For simplicity, the boat was not able to make a turn. Since the output of the boat is thrust and not velocity, a PID was added to control the velocity of the boat.

Wire

A key strength in the AGX simulation is the advanced wire simulation, and it's also easy to implement. For this simulation, the wire was used to connect the Towed-ROV to the boat. The wire in the simulation was set to the same buoyancy as our real tether cable, slight positive. Setting the right density has a lot of impact on the ROV. If the wire has big negative buoyancy, the wire and the ROV will sink, and if it has a big positive buoyancy, the ROV won't be able to dive.

PID

The PID controller using in the AGX simulation is the same as in the Towed-ROV and is written by Brett Beauregard. Since the code was original written in C++, it needed to be translated to work in python. Also, the code was found translated[8], but was not working. Therefore adjustment was made to this code to get it correct. Since the PID controller code was short and easy to translate, it was translated instead of using a python wrapper.

This PID is used to control the ROVs depth and trim as well as the velocity of the boat.

Sea

A sea to simulate the ROV in has to be created and was implemented by using a large box, with a material with the density of seawater. To add hydrodynamic to the simulation, a "WindAndWaterController" was made from AGX library. To prevent the ROV to drop bellow the seafloor, a plane at the bottom was made.

Chapter 3

Result and discussion

3.1 Mechanical design

3.1.1 ROV body

Water resistance and construction results

The ROV body was waterproof in the towing tank test and the sea pressure test. The wing shaft system, welding and flanges have successfully kept seawater from entering. However, some seawater was discovered in the camera housing after the sea pressure test when sinking the ROV 20m for ten minutes. The camera housing is separate from the ROV body. The cork gasket was replaced with a high durability silicone sealant. There has not been any leakage since. The hardened epoxy on the cable penetrations that we poured ourselves was functional, but seem brittle. The glue on threaded rods for the side plate attachment loosened after the first sea trial.

Water resistance and construction discussion

Having a waterproof ROV body straight from production was naturally practical. The silicone sealant makes opening the camera housing flange more time consuming and complicated. However, the need for opening has not come yet. The camera housing is still easily removable and different camera solutions can be tested. An epoxy intended for underwater cable penetrations should be used in future projects. The glue that kept the side plates threaded rod attachment in place is suspected to not be suitable for a wet and salty environment due to the change to a crumbling texture after the first sea trial. The sea trials went on without side plates, and no worsening of performance could be detected. Since we don't want aluminium

threads, we would need to thread a socket internally, weld it to the body, and then have stainless threaded rods for side plate attachment. The ROV as it was used during the majority of sea trials is shown in figures 3.1, 3.2 and 3.3.

Figure 3.1: ROV front.

Figure 3.2: ROV side

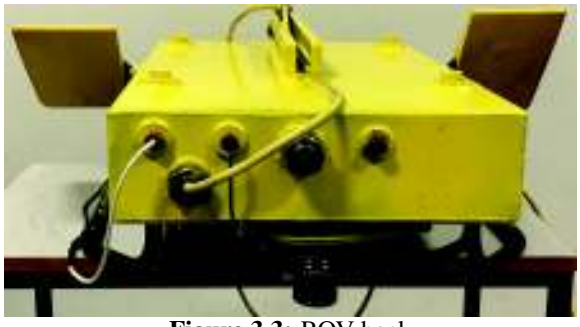

Figure 3.3: ROV back

Hydro dynamic results

The towing cable was attached above the centre of mass when the ROV was tested for the first time. The ROV kept rolling around and was too unstable at the surface. Moving the shackle as far forward as possible made it stable at the surface. The ROV kept returning to the surface upside down after almost every dive. Two 4kg steel shafts were zip-tied to the legs, but it kept turning. A PVC pipe D=40mm, L=400mm was filled with construction foam and zip-tied to the towing cable's attachment point and the ROV never turned since then.

Hydro dynamic discussion

Since the previous ROV was in no condition to be tested, it's difficult to conclude any improvement's in the new design's hydrodynamic properties. However, we assume the operating is more predictable than the previous ROV due to the less complicated and more compact shape. Constructing a waterproof and quickly built body was prioritised. Plans to add a glass-fibre nose in the front with a more hydrodynamic shape was not implemented after the camera placement turned out to be more practical in the front, and the camera needed a separate and fairly big enclosure. Early in the design process, it was planned to split a pipe lengthwise and use the rounded shape instead of a plate in the front. A pipe in a functional dimension was not in stock at NTNU Ålesund. Checking with local companies for a suitable pipe dimension should have been done. The water jet cutting could customize the port and starboard plates to a suitable fit inside the inner radius of the pipe resulting in a better design. The constructing would not be more complicated or time-consuming, and a socket could still have been welded in the front. Testing to see if the two 4kg shafts can be removed without the ROV flipping should be done in a future test. The added buoyancy of the PVC pipe should be transferred to a more permanent solution.

3.1.2 Wings and Transmission

Wings and Transmission results

The attachment between the motor shaft and the 3D-printed gear rack broke easily when stress testing by hand. The solution was to print the gear racks with a 10mmx3mm square hole, and a steel plate was fitted inside. Slipping between the shafts M6 nut and the gear occurred at higher loads. Spiked washers were tried, but there was also then not enough friction to keep the gear from slipping. When glue was applied between washer and gear, the slipping stopped. After fixing these to problems, the transmission system worked as planned. Mounting, dismounting and adjusting ratio is simple. Based on sensor data the motors are stalling at various depths. The wings weight are nearly neutral in the water.

Wings and Transmission discussion

3D-printed gear racks worked well in both PLA and PETG as material. To have a 3D printed gear on the shaft is worth trying to see if casting is necessary. We don't think 3D-printed gears can cope with the compressing stress needed to rely on friction to stop slipping. However, glue between washer and the polyurethane gear is not an acceptable solution. The need for glue is a result of prioritizing fast and uncomplicated machining, and that the polyurethane casting is very smooth. A new shaft should be machined. Keyways in the shaft dimensions we are operating

in have a height and with of 2-4mm, which requires very fine tools and tolerances. We also assume that 3D-printed gears can't cope with the shear stress in a keyway solution. A shaft milled to an octagon or similar shape at the gear seat, and a fitting gear print with an increased wall thickness should allow for 3D-printed gears on the shaft also. Figure 3.4 shows the mounted gears.

Figure 3.4: Gears and motor

A vital part in the procedure when mounting gears is to dismount the motor shaft from the gear rack, so that the new gear can be fitted whilst feeling the resistance on the wing flange while adjusting the four nuts holding the system in place. Having problems with slipping, we frequently needed to make adjustments to gears. At one point, we needed to make adjustment outside on a pier without the 8mm key needed to dismount the motor shaft from the gear rack, which resulted in a mount with a lot of added friction on the gear system. This caused a worsening of performance in that day's remaining sea trial. When we returned to NTNU Ålesund, we measured the torque by adding weights to the bolt hole of the wing flange. We found that port and starboard wing shaft was rotating with a torque of 1.9 Nm and 1.5Nm, respectively. When adjusting to a better fit, both shafts torque is measured to 1.9 Nm before stalling. This is the torque that should be used in future calculations.

Figure 3.5: Weight test

When using the largest gear possible for the ROV size, the shafts torque output was 1.9 Nm when the motor's steps/sec were reduced from 125 to 50. If the motor's force in relation to steps/sec graph provided from supplier is correct, it suggest that our transmission system's efficiency is 59%. The motors actual power must be tested in the lab when work on the ROV continues. We are concluding that the motors are powerful enough for this prototype, but more care should be put in wing design. Wings that are nearly weightless in seawater is an advantage simply due to the fact that a force is eliminated. However, the plans to make and test several wings failed due to the time spent making them, and need for a lot of polyurethane. Power and wing calculations should have been done early in the project. More precision should have been implemented in the wing construction, making sure the shaft was placed in the centre of volume. Making a spreadsheet for wing dimensioning should be made for constructing wings suitable for a number of speed ranges.

3.2 Hardware

The stepper motors seems to be good enough for adjusting the wing angles. However, we might need to reduce the speed to reach a higher torque. The reduction in speed will inflict the response of the ROV. However, this can be compensated by changing the wing design. An alternative for stepper motors can be brush less DC linear actuators.

3.2.1 Test of Kalman filter in water-tank

As a result of the sea trail where we did not get time to test the Kalman filter, a test in the water-tank at NTNU Ålesund was performed. Tuning the filter gave a good result. However, as the error variance changes with depth. The filter should be tuned at a greater depth when possible.

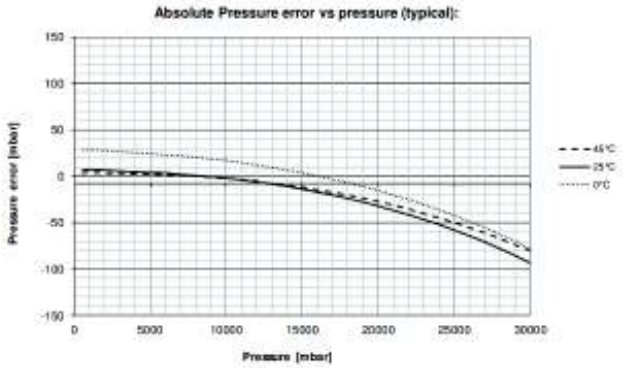

Figure 3.6: MS5837-30BA pressure error

The result, as seen in figure 3.7 show that the Kalman filter had a good effect. It's worth mentioning that the pressure read from the sensor has been set to a resolution of 1 millibar. This will make the unfiltered plot look low on resolution, compared to the Kalman filter, which on the other hand, uses a resolution of 0.01 millibar.

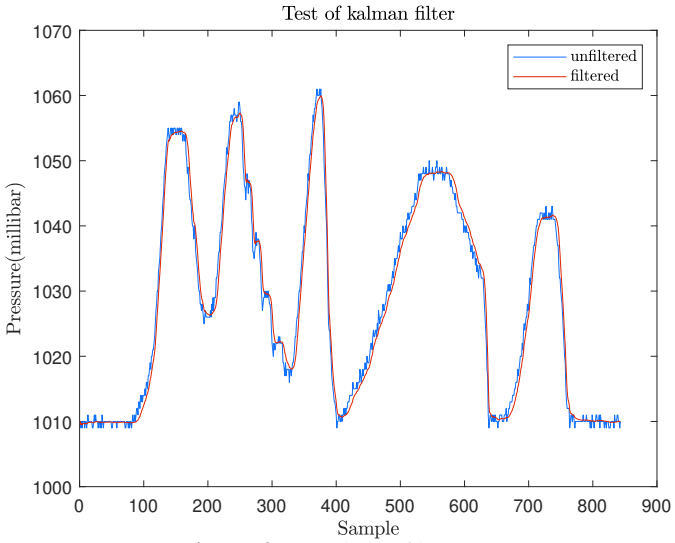

Figure 3.7: Kalman filter test

When the ROV was laying still as in figure 3.8 a lot of noise was avoided, if the resolution of the sensor were set to it highest(0.2 millibars), the noise would increase. Therefore the resolution act likes a filter in this case.

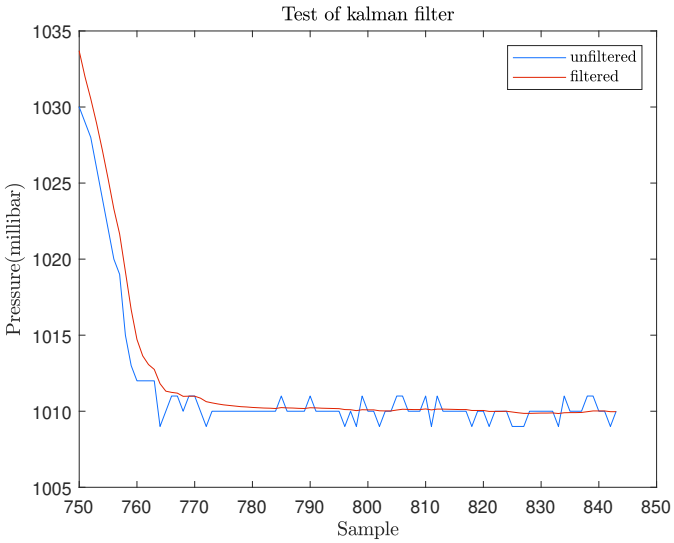

Figure 3.8: Kalman filter laying still

3.2.2 Camera result

Due to the leak in the camera house during the first test, the camera was dried for a couple of days and retested in the lab. Prior to the sea-trial the camera stopped working, and troubleshooting the camera was not prioritised. Therefore the sea-trial was executed without video. In the lab, after sea-trials the camera was troubleshooted, and as we knew that the camera worked occasionally, the soldering between the USB connection and camera cable was replaced with a screw terminal. This lead to the camera operating again. In figure is an image from a test performed in the water-tank to test the image quality underwater in low light. Since one of our light was leaking the light has been disconnected and a smartphone flashlight was used. The quality of the image from the water-tank test can be seen in figure 3.9. The wrench is approximately 1.2 meters away from the camera, and this disappears approximately three meters from away.

Figure 3.9: Camera test in water-tank

3.2.3 Camera Discussion

Since the camera has limited test in low light, to conclude if the camera is adequate for its purpose is difficult. The limited test in the water-tank indicates that the two currently mounted lights are not sufficient to get a good image. Also keeping in mind that the wrench is quite reflective. Furthermore the plastic bulb had got some scratches from moving the ROV around, which in good light conditions limits the image quality. Since plastic is a soft material, some protective to the bulb should have been made.

3.3 Control system

The results are as expected mixed as we had a practical approach in this project due to the amount of work. However, we believe this was the right approach as we got results and have had enough time to evaluate them.

3.3.1 Depth control

The graph in figure 3.10 displays the relationship between the setpoint and measured depth. The resolution on the graphs is 0.1 meters for depth and 1 degree for pitch and wing position. Table 3.1 contains some values describing the ROVs response. It appears that the system's behaviour is similar when diving and ascending.

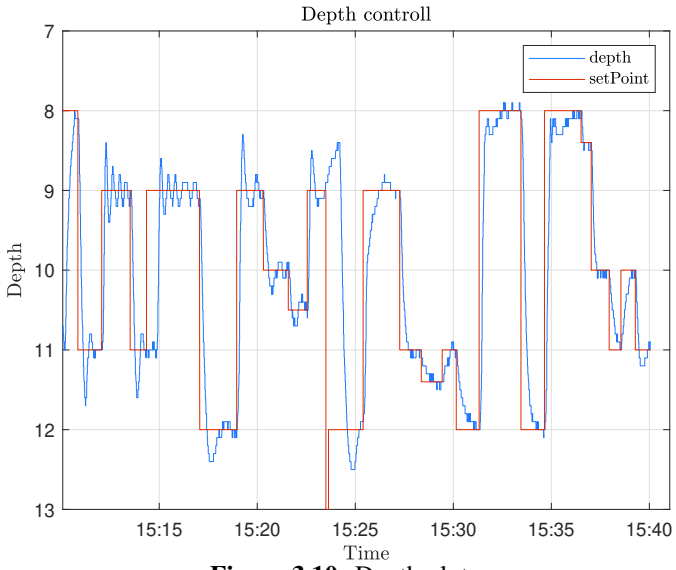

Figure 3.10: Depth plot

Table 3.1: System response

Nr.	Change SP(m)	tau(s)	TR(s)	TP(s)	%OS	TS(s)	[kp ki kd]	Time graph
1	11-9	5.6	5.4	13.0	30	N/A	[10 3 3]	15:12:04
2	12-8	12.2	10.6	N/A	N/A	55.9	[30 1 0]	15:31:19
3	8-8.4	4.5	N/A	N/A	N/A	6	[30 1 0]	15:36:31
4	8.4-10	5.4	7.2	N/A	N/A	17.1	[30 1 0]	15:37:02
5	10-11	13.4	23.7	N/A	N/A	30.4	[20 2 0]	15:37:57
6	11-10	13.7	23.6	N/A	N/A	31.7	[20 2 0]	15:38:33

Figure ref displays the relation between pitch, wing angle, and depth. The behaviour of the wings is different when comparing diving and ascending. We believe this is because the pitch angle is not taken into account when setting the wing angle. Resulting in varying wing angles relative to the sea surface.

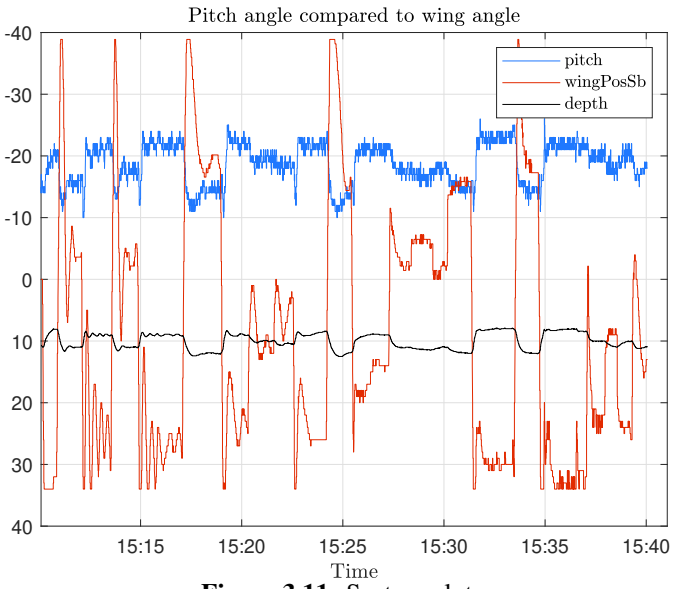

Figure 3.11: System plot

3.3.2 Roll control

The roll angle is quite unstable. Figure 3.12 indicates that the roll angle decreases as the depth increases. When the change in depth is settling, the roll angle varies with about $\pm 5°$.

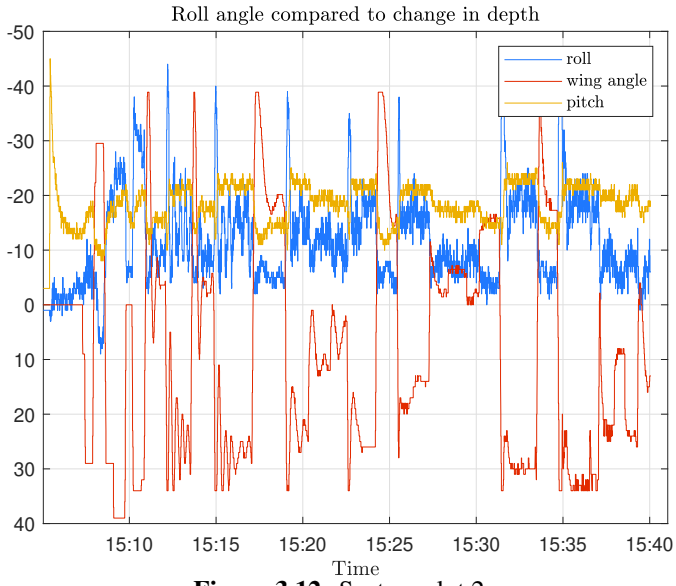

Figure 3.12: System plot 2

The reason we tested without the trim controller was an error in the Arduino code. When sending the wing position to the GUI, the same variable was used for both wings. Resulting in equal wing angles in the GUI. As we did not see any reaction in the GUI when turning on the trim controller, we turned it off. However, we believe the main reason for the high roll angle is the inequality in the wing positions due to missed steps by the stepper motors.

After discovering the error in the Arduino program, we tested the trim response in the lab. Figure 3.13 displays the wing angle response to different roll angles.

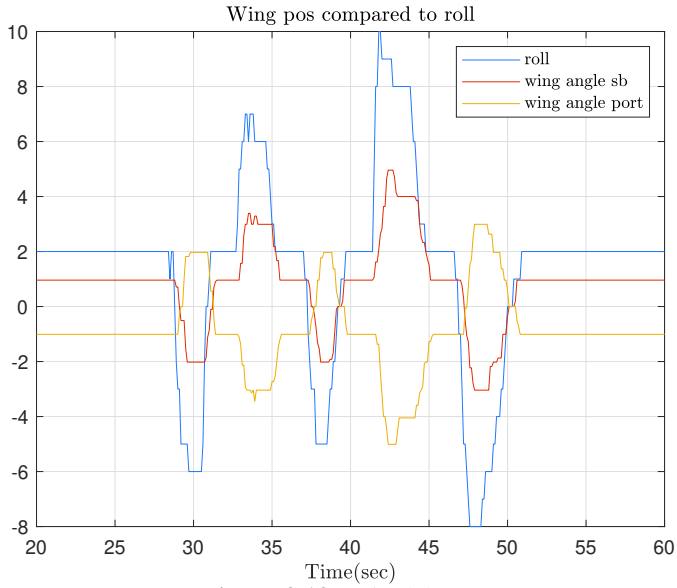

Figure 3.13: Trim lab test

3.3.3 Controller discussion

We did not get as much time testing the system as we would like to. There are several reasons As the school had no boat available we had to go to Hellesylt where we could lend one. Then we got some problems with the outboard motor, leaving us with no boat for four days. We spent the time making some changes, and it also gave us some more time to work on the simulation. With that being said, we should have done more testing on land before the sea trials. This would most likely prevent some of the basic errors, making the sea trials more effective. However, the results we got have made us aware of several things. Some of them were fixed, while others will be discussed in this section.

We believe that a PID controller is well suited to control the ROV from the results we got. Due to the limited time, we did not find an optimal tuning. However, we got to know the ROV better and found a decent controller with a fast transient response and no overshoot. The steady-state response was slow but stable. These characteristics should be well suited for seafloor tracking, as the transient response would let the ROV avoid obstacles, while at the same time keep it stable when closing in on the setpoint. With some more tuning, the settling time could probably be reduced.

The small range that the ROV operated in, is most likely more linear then a wider range would be. Meaning an increased range could cause problems for the linear PID controller. If this is the case, a fuzzy system controlling the parameters could

be implemented. We chose to not implement it at this stage, as we did not have enough experience with the system, and the fact that a simple PID was sufficient for now.

For the ROV to go deeper there are mainly three changes that could increase the range. By extending the length of the rope, the force pulling the ROV will be less effective pulling it up as the angle between the ROV and the rope decreases. Adding a trim spoiler giving a greater pitch would make the ROV go deeper as well (FIKS setting trqq). The last improvement would be to either optimize the use of the current wings by taking the pitch angle into account and possibly build new more effective wings.

Figure 3.10 and table 3.1 describes the response of the ROV. As the system behaves similar when diving and ascending, we believe that the positive buoyancy of about 130N is not an issue.

We made a mistake by setting the resolution for depth to 0.1 meters and did not notice it until after the sea trial. A higher resolution would have given a better view of the ROVs actual movement. Although it probably did not affect the controller too much. It would give the ROV a better steady-state response, as the controller would not react until it is 0.1m off.

We noticed that a PI controller seems to perform better than a PID controller as the system is relatively slow. By setting KP to 30 and KI to 1 we got a decent result. With a good rise time and no overshoot, while the settling time could have been better. However, for an increased range, the derivative could possibly be useful.

There are some issues with the roll angle. We believe most of the reason is the trim angle caused by the motors skipping steps. Another factor can be that the centre of buoyancy and mass is not on the same point. By adding some weight at each of the feet and a small pipe in the centre on top of the ROV, the roll angle became better. This must be looked more into. Filling the ROV with oil and adding some buoyancy at the top could be a more permanent solution. Especially if the ROV operates below 40 meters.

3.4 Simulation

Note, all plots of pitch are oscillating at the beginning of the simulation. Also, the wing angle is oscillating due to the stiffness of the simulated system had to be softened to be able to run on our computers. Meaning the connection point of the hinge can differ a bit.

3.4.1 Simulation result

At the same velocity (3.5 knots) and density as the real ROV, the simulation is not able to control the same way. This is displayed in figure 3.14. The result shows that it's limited to 9 meters, although this can be compensated with a longer wire. On the other hand, the pitch is over 45 degrees, meaning that when the wings are at the max positive position, it will point slightly down and not give any lift. As mentioned in section 2.3.5, the wings have no lift at $0°$ therefore if the pitch gets too large, it's not possible to control the pitch. Since max wing angle will be perpendicular to the flow of the water when pitch reaches $45°$.

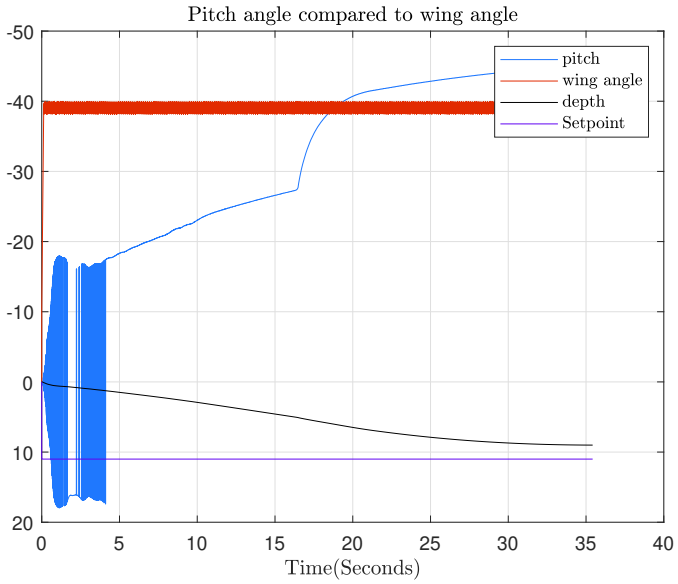

Figure 3.14: Simulated depth control at 3.5 knots

After experimenting with speed, it was found that 11 knots will give a response where it can be controlled around the same depth as the real ROV. The result from a simulation is shown in figure 3.15 and 3.16.

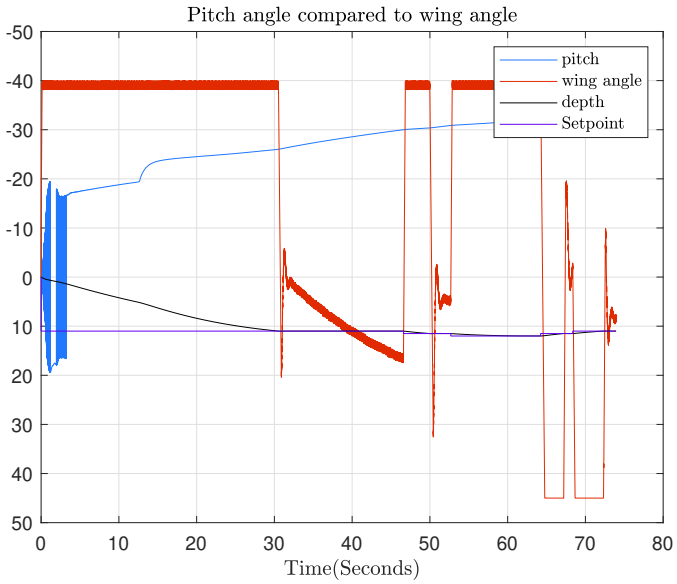

Figure 3.15: Simulated depth control at 11 knots

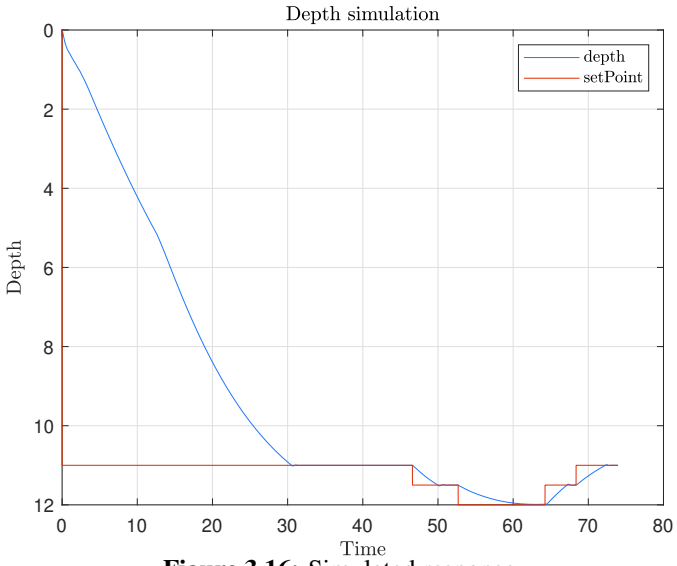

Figure 3.16: Simulated response

Solid model simulation

An ROV with a non-hollow body was tested, and the result is shown in figure 3.17. This test was done at 10 knots, but the model was tested at 5, 10, 20 and 30 knots. At 10, 20 and 30 the ROV was not able to dive beneath 5.8 meters. At 5 knots the ROV was only able to dive 2,4 meters. A manual test of the ROV at 10 knots was also completed, this was to see the change in pitch of the ROV when changing

wing angle. The result is shown in figure 3.18, where there is a slight response when changing the wing angle.

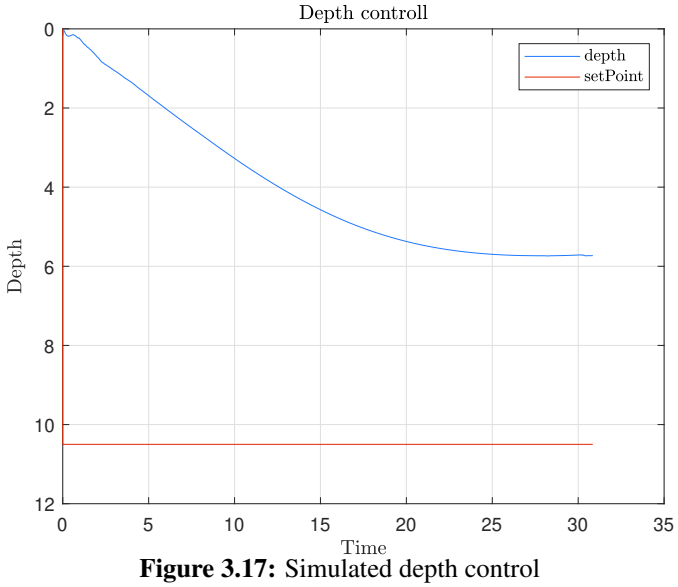

Figure 3.17: Simulated depth control

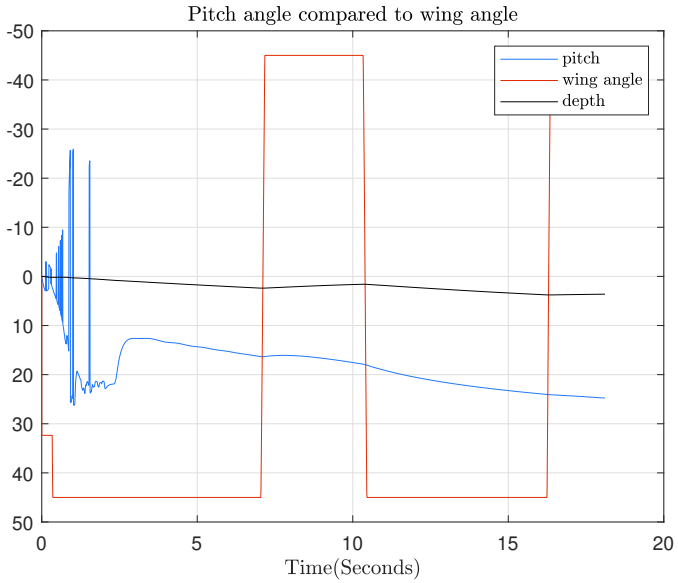

Figure 3.18: Simulated manual pitch

Trim PID

The result from the trim PID is shown in figure **. It shows that the PID is able to keep up with the roll of the ROV until the output was maxed within the set limit of $\pm 8°$. It was also tested with a larger output limit, with the same results.

Stability of model

As a result of the trim, PID was not able to control the ROV with a range of $\pm 8°$, the stability of the model was tested. Figure 3.19 shows the roll of the ROV towed behind the ROV without wings. It shows that the model will eventually roll over after time. Note, this test will also take in the inaccuracy placement of the towing cable on the ROV. Therefore the placement of the towing cable was moved around without any big changes in the long term behaviour. The velocity of the ROV in this test was set to 11 knots.

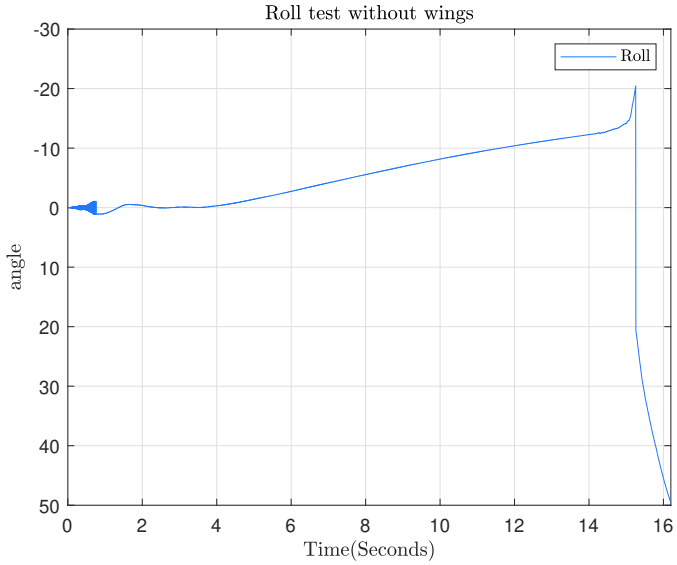

Figure 3.19: Simulated stability without wings

Figure 3.20 shows the roll of the ROV body towed behind another ROV with wings (no angle). As in the test without wings the rov will eventually roll over as well.

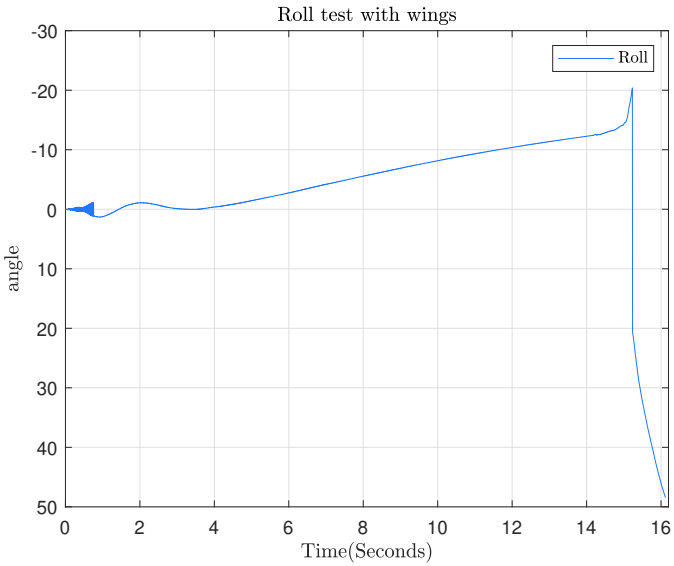

Figure 3.20: Simulated stability with wings

3.4.2 Simulation discussion

Simulation vs real ROV

The result shows clearly that there is a deviation with the simulation compared to the sea-trials. It more specifically shows that a higher speed is required to achieve reasonably equal response as the real. It's most likely a mix of reasons why the simulation differs, and we need to keep in mind the complexity of the system. One part can be that there is no current in the water since the current will differ it has been neglected. Also from the result from sea-trial show no big change when dragging with or against the current. Another maybe as explained in section 3.4.2 that the model simulated is hollow and therefore filled with water. As the simulation differs from the real ROV, it is not yet possible to tune the real ROV by using the simulator. In addition to the differ in velocity, the rate of change in pitch and the amount the pitch differ is a deviation from the sea-trial. From the result we saw that the pitch differ less as well as the rate of change was lower. This leads to that further test on different wings, position on wings, side-plates, spoiler etc will not be accurate. Although, it can be used to get a general idea of the change in the system.

At around 5 meters of depth the pitch have a rapid change in pitch angle, this is due to the rope tightening up after an rapid acceleration from the boat.

Trim

The result of the PID trim test can be looked at successful. Although it was not able to control it over time. This is probably due to the asymmetry in the simplified model. It can also be that the actual model have a center of buoyancy and a center of gravity off center, making the ROV roll around.The ROV rolling around was also a problem during sea-trial but was fixed with weights and a pipe (with positive buoyancy), this will move the centre of buoyancy and gravity to the centre. This has not been implemented in the simulation. From figure 3.12 we can see that the ROV is always tilting the same way as the ROV in simulation is rolling. This strengthen the case that center of buoyancy and gravity is shifted off center.

The reason behind we can say the test was successful is that the PID was able to control the ROV as long as the forces from asymmetry of the model were not bigger than the wings could compensate. The result shows no big changes when moving the cables point of attachment on the ROV as well as the position of the wing. Therefore the most likely reason for the ROV rolling is either the asymmetry of the actual mode, the asymmetry of the simplified model or a combination.

Solid ROV body

After not getting the correct result from the model used in result, it was discovered that the wind and water controller in AGX only calculated the hydrodynamic on one side of a triangle in a mesh. This meant the hollow ROV body (section) was filled with water, this has an impact on the simulation. It was therefore made solid and not hollow. In theory, this should be a more accurate model, although the result showed that either the velocity of the boat, the ROV could not get below 5.8 meters of depth. It had been discovered during the sea-trial that it was the ROV body that affected the depth the most, it is therefore important that pitch was close to the one as sea-trial. If we compare the hollow model with the solid, we do not see any big difference in pitch, meaning the wing angle have the same effect. On the other hand the to set the correct density the hollow model is bit bigger, but it makes also the body and wings bigger. Mainly its the hollow body filled with water that gives an effect. The solid body should be in theory be a more accurate model, but with limited time using the model with the more accurate response was choose to use for further tests.

Bibliography

[1] B. Prakash M. Mofidi. Frictional behaviour of some sealing elastomers in lubricated sliding conditions. Accessed:2020-11-19.

[2] Jarle Johannessen. *Tekniske tabeller*, volume 1. cappelen, second edition, 2002.

[3] DNV. Environmental conditions and environmental loads.

[4] Gary Bishop Greg Welch. An introduction to the kalman filter.

[5] Sea science, the acrobat. https://www.seasciences.com/physical-description/?fbclid=IwAR3tbZmFyY7PrurDseWnllQX0ivA-8Dtpj79JpKB2Wb20c-BnKv-jDs04D0. Accessed: 2020-11-20.

[6] Ping sonar, echo sounder. https://bluerobotics.com/store/sensors-sonars-cameras/sonar/ping-sonar-r2-rp/. Accessed: 2020-11-12.

[7] Agx dynamic documentation. https://www.algoryx.se/documentation/complete/agx/tags/latest/UserManual/source/index.html. Accessed: 2020-11-18.

[8] simple-pid. https://pypi.org/project/dvg-pid-controller/#description. Accessed: 2020-10-24.

3.5 Appendix

3.5.1 Shematics

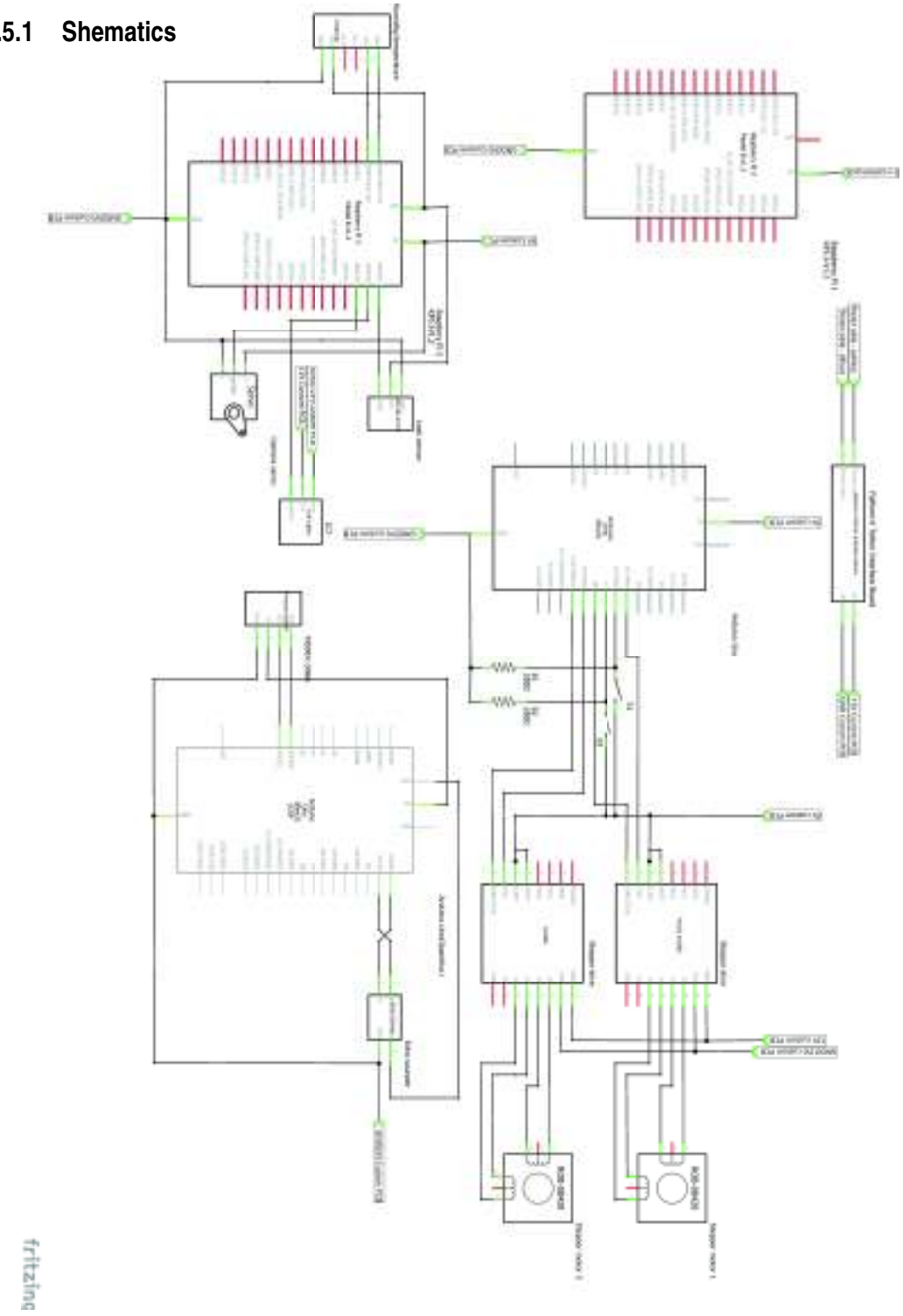

3.5.2 Technical drawings

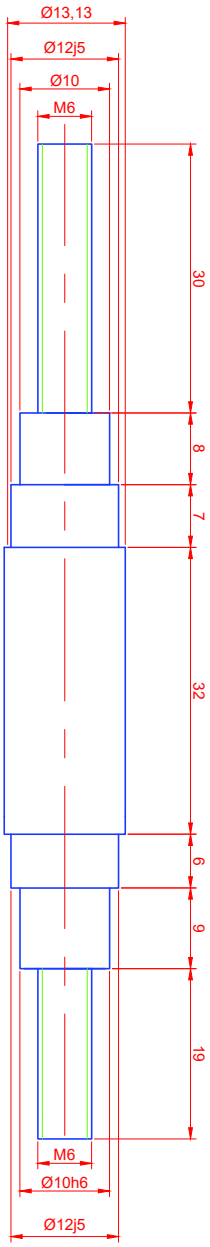

For ikke toleransesatte mål: NS-ISO 2768-1 middels

Utvendige hjørner fases 1x45°
Max radius på 0,3mm alle innvendige hjørner

Slå gjenger med gjengebakke så langt som mulig

Antall pr. enh.	2			
Pos. nr		Navn, type, dimensjon	Aksel	
Dato	18.09.20	Konstr/Tegnet	E.M.	
Kontroll		Standardnr.		
		Godkjent		Tracet
		Prosjeksjonsmetode		Målestokk 4 : 1
Tegning Produktnr.			0004	
Materiale			rustfri/syrefast	
Kg pr. stk.				
Kjennemerke				

NTNU
Pod-Skip

Aksel

0004

Henvisning
Beregning
Gruppe
Erstatning for:
Erstattet av:

3.5.3 Technical drawings

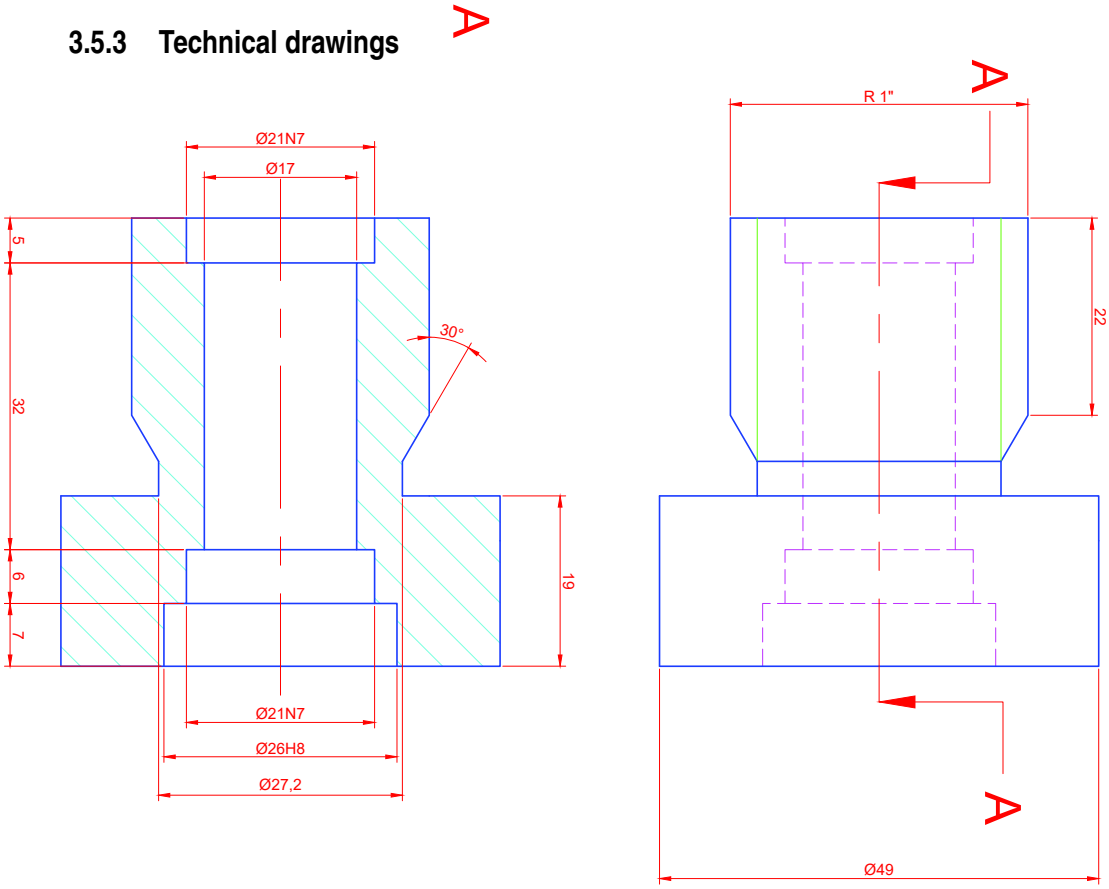

For ikke toleransesatte mål: NS-ISO 2768-1 middels

Utvendige hjørner fases 1x45°
Max radius på 0,3mm alle innvendige hjørner

Antall pr. enh.	2	Navn, type, dimensjon	Gjennomføring	
Pos. nr.		Tegning Produktnr.	0002	
Materiale	ALU	Kg pr. stk.		Kjennemerke
Dato	18.09.20	Konstr./Tegnet	E.M.	Trace
Kontroll		Standkontr.		Godkjent
Målestokk	2 : 1	Prosjektjonsmetode		

NTNU
Pod-Skip

Erstatning for:
Erstattet av:

Henvisning
Beregning
Gruppe
0002

Gjennomføring

PRODUCED BY AN AUTODESK STUDENT VERSION

3.5.4 Technical drawings

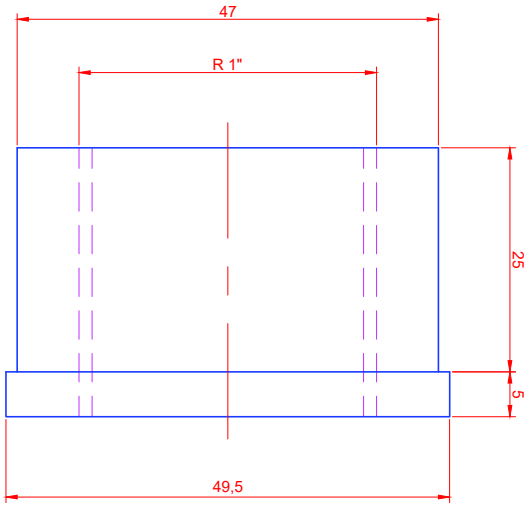

NS-ISO 2768-1 middels
Utvendige hjørner fases 1x45°

Antall pr. enh.	2	Navn, type, dimensjon	Muffe	Tegning/ Produktnr.	0003
Pos. nr.				Materiale	ALU
Dato	18.09.20	Konstr./Tegnet	E.M.	Målestokk	2: 1
Kontrollt		Standardnr.		Godkjent	
Trace		Prosjektjonsmetode		Kg pr. stk.	
Erstatning for:		NTNU Pod-Skip		Kjennemerke	
Erstattet av:					
Gruppe	0003				
Beregning		Muffe			
Henvisning					

PRODUCED BY AN AUTODESK STUDENT VERSION